nature cell biology

ARTICLES

Auxin regulates aquaporin function to facilitate lateral root emergence

Benjamin Péret[1,6,7], Guowei Li[2,7], Jin Zhao[3,7], Leah R. Band[1,7], Ute Voß[1], Olivier Postaire[2], Doan-Trung Luu[2,6], Olivier Da Ines[3,6], Ilda Casimiro[4], Mikaël Lucas[1], Darren M. Wells[1], Laure Lazzerini[1], Philippe Nacry[2], John R. King[1], Oliver E. Jensen[1,5], Anton R. Schäffner[3,8], Christophe Maurel[2,8] and Malcolm J. Bennett[1,8]

Aquaporins are membrane channels that facilitate water movement across cell membranes. In plants, aquaporins contribute to water relations. Here, we establish a new link between aquaporin-dependent tissue hydraulics and auxin-regulated root development in *Arabidopsis thaliana*. We report that most aquaporin genes are repressed during lateral root formation and by exogenous auxin treatment. Auxin reduces root hydraulic conductivity both at the cell and whole-organ levels. The highly expressed aquaporin PIP2;1 is progressively excluded from the site of the auxin response maximum in lateral root primordia (LRP) whilst being maintained at their base and underlying vascular tissues. Modelling predicts that the positive and negative perturbations of PIP2;1 expression alter water flow into LRP, thereby slowing lateral root emergence (LRE). Consistent with this mechanism, *pip2;1* mutants and *PIP2;1*-overexpressing lines exhibit delayed LRE. We conclude that auxin promotes LRE by regulating the spatial and temporal distribution of aquaporin-dependent root tissue water transport.

The establishment of a mature root system is achieved through repetitive branching of the primary root. This process—called lateral root formation—is initiated deep within the primary root from a small subset of pericycle cells[1]. The growth of a new LRP coincides with its emergence through the outer tissues[2]. The tight coordination of lateral root formation and emergence is controlled by auxin[3,4], which acts as a local inductive signal and favours cell separation in the overlaying tissues[5].

The biomechanics of LRP growth and its potential link with auxin are only partially understood[5]. In particular, the role of tissue water transport during LRE has not been examined. In addition to the formation of new cells, plant tissues grow when cell walls relax and extend in response to the cell's turgor pressure[6]. Sustained growth is primarily driven by solute uptake and maintenance of cell osmotic potential, and requires sufficient water inflow to keep turgor above yield threshold[7]. The water needed for growth is typically supplied either through the vasculature or the soil, before being transferred from cell to cell[7]. Therefore, the hydraulics of the whole plant or expanding tissues can be critical[8,9]. Although water transport is known to affect growth of leaves and primary roots[8,10], its significance during LRE has not been explored. Yet, the LRP is symplastically isolated from the primary root vasculature[11], suggesting the need for efficient transcellular water fluxes towards the dividing and expanding cells.

Aquaporins represent a large class of membrane channels present in most living organisms[12]. In plants, aquaporins fall into seven subfamilies[13], which include plasma membrane intrinsic proteins (PIPs) and the tonoplast intrinsic proteins (TIPs). Their role in plant water relations has been studied and linked to a wide range of functions[14,15], including root water uptake and regulation of tissue hydraulic conductance under environmental stresses.

To address the hydraulics of LRP growth and emergence, we studied the role of aquaporins during early stages of lateral root development

[1]Centre for Plant Integrative Biology, University of Nottingham, LE12 5RD, UK. [2]Biochimie et Physiologie Moléculaire des Plantes, Institut de Biologie Intégrative des Plantes, Unité Mixte de Recherche 5004 Centre National de la Recherche Scientifique - Unité Mixte de Recherche 0386 Institut National de la Recherche Agronomique - MontpellierSupAgro - Université Montpellier 2, 2 Place Viala, F-34060 Montpellier Cedex 2, France. [3]Institute of Biochemical Plant Pathology, Helmholtz Zentrum München, 85764 Neuherberg, Germany. [4]Universidad de Extremadura, Facultad de Ciencias, Badajoz 06006, Spain. [5]School of Mathematics, University of Manchester, M13 9PL, UK. [6]Present addresses: Unité Mixte de Recherche 7265 Commissariat à l'Energie Atomique et aux Energies Alternatives, Centre National de la Recherche Scientifique, Laboratoire de Biologie du Développement des Plantes, Université d'Aix-Marseille, 13108 Saint-Paul-lez-Durance, France (B.P.); Université des Sciences et Techniques de Hanoï, Institut de Recherche pour le Développement Laboratoire Mixte International Rice, Agronomical Genetics Institute, Ha Noi, Vietnam (D-T.L.); Génétique, Reproduction et Développement, Unité Mixte de Recherche 6293 Centre National de la Recherche Scientifique, Institut National de la Santé et de la Recherche Médicale U1103, Université de Clermont-Ferrand, Aubière 63170, France (O.D.I.). [7]These authors contributed equally to this work. [8] Correspondence should be addressed to A.R.S., C.M. or M.J.B. (e-mail: schaeffner@helmholtz-muenchen.de or maurel@supagro.inra.fr or malcolm.bennett@nottingham.ac.uk)

Received 28 June 2011; accepted 8 August 2012; published online 16 September 2012; DOI: 10.1038/ncb2573

in *Arabidopsis*. We observed that most aquaporin genes are repressed during lateral root formation in an auxin-dependent manner. As a result, auxin represses root cell hydraulic conductivity. We describe how auxin-related changes in aquaporin distribution may be important for organ emergence and provide converging mathematical and genetic evidence that aquaporins facilitate LRE. Our results demonstrate a complex spatial and temporal interaction between auxin and aquaporin function, to support LRP growth.

RESULTS

Most aquaporin genes are repressed by auxin during lateral root formation

We initially considered whether aquaporin expression was altered during lateral root development. Lateral root initiation can be induced by either mechanical[16,17] or gravitropic[18,19] stimuli. Following a 90° gravitropic stimulus, lateral roots develop in a highly synchronized manner at the outer edge of a bending root (Fig. 1a,b). Stage I primordia[20] were first detected 18 h post-gravitropic induction (pgi); then primordia for each subsequent stage were detected approximately every 3 h, until emergence at stage VIII, ~42 h pgi (Fig. 1b). We profiled aquaporin gene expression during lateral root development at high temporal resolution (that is, at every stage of lateral root development) by micro-dissecting root bends every 6 h pgi.

Profiling all 13 PIP and four highly expressed TIP isoforms by real-time quantitative PCR with reverse transcription (RT–qPCR) revealed that 14 of the 17 genes were repressed during lateral root development whereas *PIP1;4* and *PIP2;5* showed no or little induction (Fig. 1c,d). In contrast, *PIP2;8* was induced up to tenfold 36 h pgi (Fig. 1d). Repression of most aquaporin genes occurred during early lateral root formation (about 6 pgi), corresponding to when auxin accumulates in pericycle founder cells[21]. However, four *PIP* genes, including the highly expressed isoforms *PIP2;1* and *PIP2;2* (refs 22,23), showed a delayed repression at >10 h pgi (Fig. 1c).

Auxin is a key signal during early stages of lateral root development[4]. Treatment of whole roots with the auxin indole-3-acetic acid (IAA) induced an overall inhibition of aquaporin gene expression (Fig. 1e). Whereas *PIP1;3* and *PIP2;4* showed up to twofold induction, the 15 other *PIP* and *TIP* genes were repressed after IAA treatment (Fig. 1e,f). Only *PIP2;5* and *PIP2;8* recovered and even overshot their previous level. The similar expression profiles following gravity and auxin treatments suggest that auxin is responsible for the repression of aquaporin gene expression during LRE. The temporal differences observed are likely to reflect the synchronous and asynchronous cellular responses to endogenous and exogenous auxin sources, respectively. Nevertheless, our results reveal that auxin represses the expression of most aquaporin genes in the *Arabidopsis* root.

Auxin controls root aquaporin expression through ARF7

Auxin response factor (ARF) proteins function as transcription factors controlling auxin-responsive genes[24]. ARF7 plays a key role during lateral root formation and emergence[5,25–28]. Thus, we determined the effects of the *arf7* loss-of-function on *PIP* and *TIP* expression. For *PIP1;1*, *PIP1;4*, *PIP2;1*, *PIP2;2* and *PIP2;7* showing sustained auxin-dependent repression, a diminution of hormone effects was observed in the *arf7* mutant (Fig. 2a and Supplementary Fig. S1). Expression of the remaining auxin-repressed *PIP* genes was similar between the two backgrounds. Interestingly, auxin induction of *PIP1;3* and *PIP2;5* was also ARF7 dependent.

Next, we investigated whether transcriptional repression of aquaporin genes by auxin resulted in reduced aquaporin protein content. Enzyme-linked immunosorbent assays (ELISAs) using an antibody specific for PIP2;1, PIP2;2 and PIP2;3 (ref. 29) revealed a strong diminution of these aquaporins in the root, to 79% and 45%, at 18 and 42 h after auxin treatment, respectively (Fig. 2b). In contrast, the *arf7* mutation counteracted the auxin-induced reduction of these aquaporins (Fig. 2b). We conclude that auxin diminishes the accumulation of these aquaporins by inhibiting their expression in an ARF7-dependent manner.

Auxin controls root hydraulics and cell turgor through ARF7

To examine the effects of auxin on aquaporin function, roots of hydroponically grown plants were treated with IAA and their water-transport properties were characterized[30]. The root water permeability measured with a pressure chamber (hydrostatic hydraulic conductivity, $Lp_{r\text{-}h}$; ref. 30) was not affected on short auxin treatments (Supplementary Fig. S2a). However, longer treatments triggered a large drop in $Lp_{r\text{-}h}$ (by up to 69%; Fig. 2c). When measured under conditions of free sap exudation[30], root water permeability (osmotic hydraulic conductivity, $Lp_{r\text{-}o}$) also showed a marked (−51%) inhibition after 42 h of auxin treatment (Supplementary Fig. S2b). Interestingly, $Lp_{r\text{-}h}$ of *arf7* was insensitive to auxin inhibition (Fig. 2c). Yet, the *arf7* $Lp_{r\text{-}h}$ was inhibited by 5 mM H_2O_2 (Supplementary Fig. S2c). This aquaporin-blocking treatment[31] demonstrates that *arf7* specifically altered aquaporin inhibition by auxin. Hence, ARF7 plays a central role in auxin-dependent regulation of aquaporins in the *Arabidopsis* root.

To determine whether auxin-dependent regulation of aquaporin function also applies to root cortical cells, the water relation parameters of these cells were deduced using a cell pressure probe[30] (Supplementary Fig. S2d–f). A drop in cortical cell hydraulic conductivity (Lp_{cell}) by 48% was observed 18 h after IAA application (Fig. 2d). A longer (42 h) auxin treatment triggered a strong reduction of cortical cell turgor, in accordance with older reports in cucumber hypocotyls[32]. In contrast, the cortical cell turgor remained constant in the *arf7* mutant (Fig. 2e). Our data indicate a dual effect of auxin on cortical cell water relations, both of which are under the control of ARF7.

Auxin alters aquaporin spatial expression during lateral root development

Our expression and functional studies suggest that auxin-regulated aquaporin gene expression may play an important role during lateral root development. To investigate this further, we focused on PIP2;1, one of the most highly expressed aquaporins in roots[22,23] that was regulated by auxin in an ARF7-dependent manner. A loss-of-function mutant (*pip2;1-2*; ref. 33) showed a decrease by 14% ($p < 0.01$) in $Lp_{r\text{-}o}$, indicating that PIP2;1 contributes significantly to root hydraulics (Fig. 2f and Supplementary Fig. S2g–j).

Expression studies using transcriptional (*proPIP2;1:GUS*) and translational (*proPIP2;1:PIP2;1–mCHERRY*) fusions revealed that *PIP2;1* is highly expressed in the stele and less in outer root layers (Fig. 3a,d,e). *PIP2;1* is expressed in stage I LRP (Fig. 3a,d), but from stage III onwards *PIP2;1* expression is excluded from LRP tips

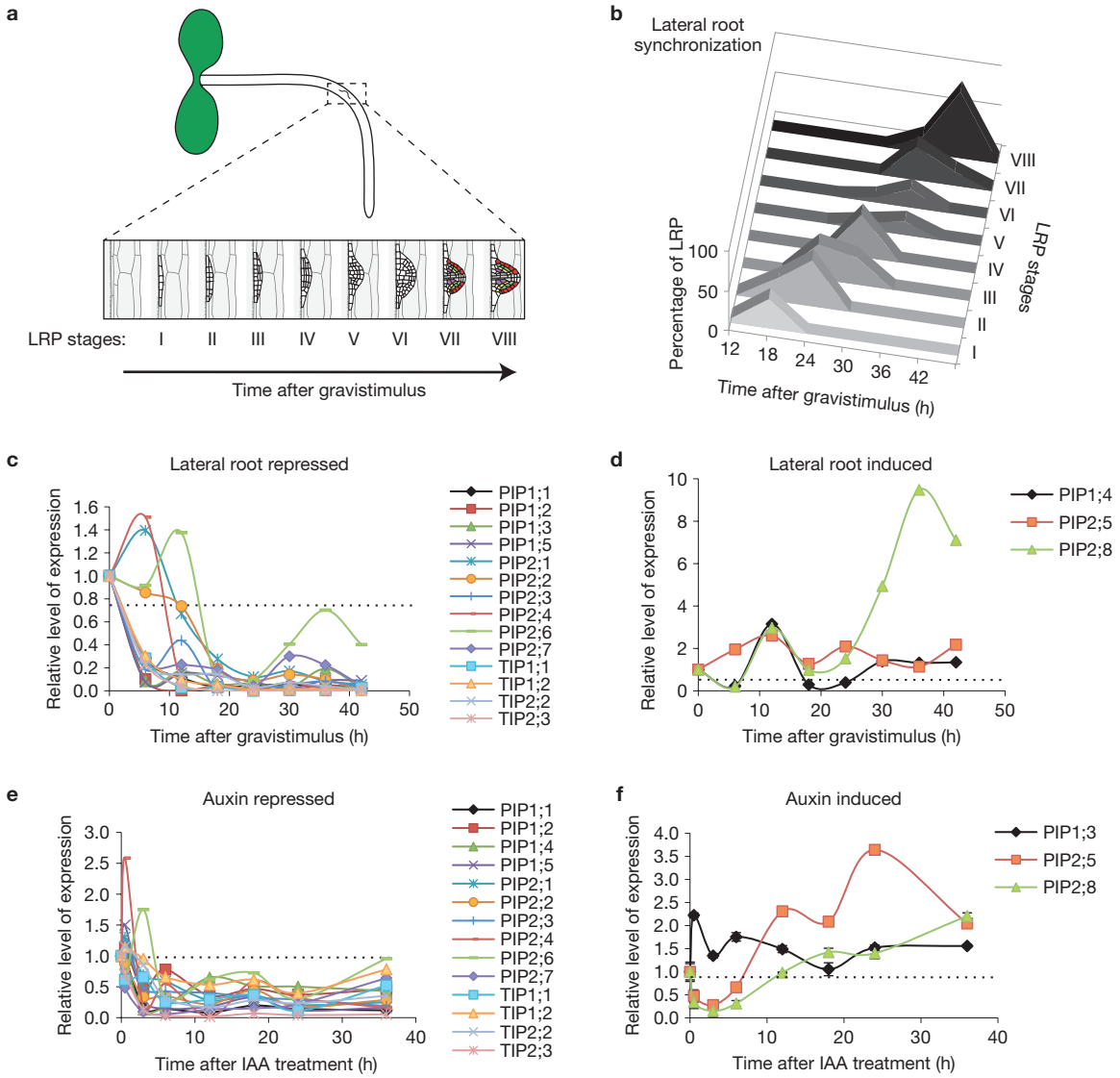

Figure 1 Transcriptional downregulation of aquaporins during lateral root formation is mediated by auxin. (**a**,**b**) Lateral root synchronization was obtained after a 90° gravitropic stimulus. (**a**) An LRP was induced at the root bend created after the stimulus according to previous reports[18]. (**b**) LRP stages (from I to VIII according to previous descriptions[20]) were determined every 6 h post-stimulus and are represented as a percentage of the total number of induced LRP. (**c**,**d**) The aquaporin gene expression level was followed after gravistimulation of lateral root formation and dissection of the root bend. The relative level of expression is shown as a function of time after gravistimulus. (**c**) Out of the 17 major aquaporin genes, 14 genes are repressed during lateral root formation (*PIP1;1, PIP1;2, PIP1;3, PIP1;5, PIP2;1, PIP2;2, PIP2;3, PIP2;4, PIP2;6, PIP2;7, TIP1;1, TIP1;2, TIP2;2* and *TIP2;3*). (**d**) *PIP1;4* and *PIP2;5* show little induction during lateral root formation whereas *PIP2;8* is induced. (**e**,**f**) Auxin generally downregulates aquaporin gene expression. The aquaporin gene expression level was determined in the whole root after treatment with auxin (1 μM IAA) for the indicated time. (**e**) 14 aquaporin genes are repressed by auxin (*PIP1;1, PIP1;2, PIP1;4, PIP1;5, PIP2;1, PIP2;2, PIP2;3, PIP2;4, PIP2;6, PIP2;7, TIP1;1, TIP1;2, TIP2;2* and *TIP2;3*). (**f**) *PIP1;3* and *PIP2;8* show little induction during lateral root formation whereas *PIP2;5* is induced. For clarity, error bars are not included in the graph. Numerical values are provided in Supplementary Table S1.

(Fig. 3b,d). This expression pattern was the exact opposite of the auxin response reporter DR5 (refs 5,21; Fig. 3c), consistent with our results that auxin represses *PIP2;1* expression (Fig. 1e,f). We also observed that auxin treatment resulted in a strong reduction of the *proPIP2;1:GUS* signal (Fig. 3e,f), whereas treatment with the auxin response inhibitor *p*-chlorophenoxy-isobutyric acid (PCIB) resulted in a strong increase of the *proPIP2;1:GUS* signal and extended the spatial pattern into the outer layers (Fig. 3e,g). Our observations suggest that auxin accumulation causes a reduction in *PIP2;1* expression in the LRP.

Expression of *PIP2;8*, which was upregulated at a later phase of lateral root development or after long exogenous auxin treatments (Fig. 1d,f) is largely restricted to the stele (Supplementary Fig. S3a–f). From stage IV onwards, *PIP2;8* expression is induced at the LRP base and underlying stele (Supplementary Fig. S3c–f) but is not altered by exogenous IAA or PCIB treatment (Supplementary Fig. S3g–m). Thus, the auxin-induced enhancement of lateral root number accounts for the apparent auxin-dependent *PIP2;8* upregulation (Supplementary Fig. S3g–i). Taken together, the *PIP2;1* and *PIP2;8* expression data suggest that lateral root development involves a fine

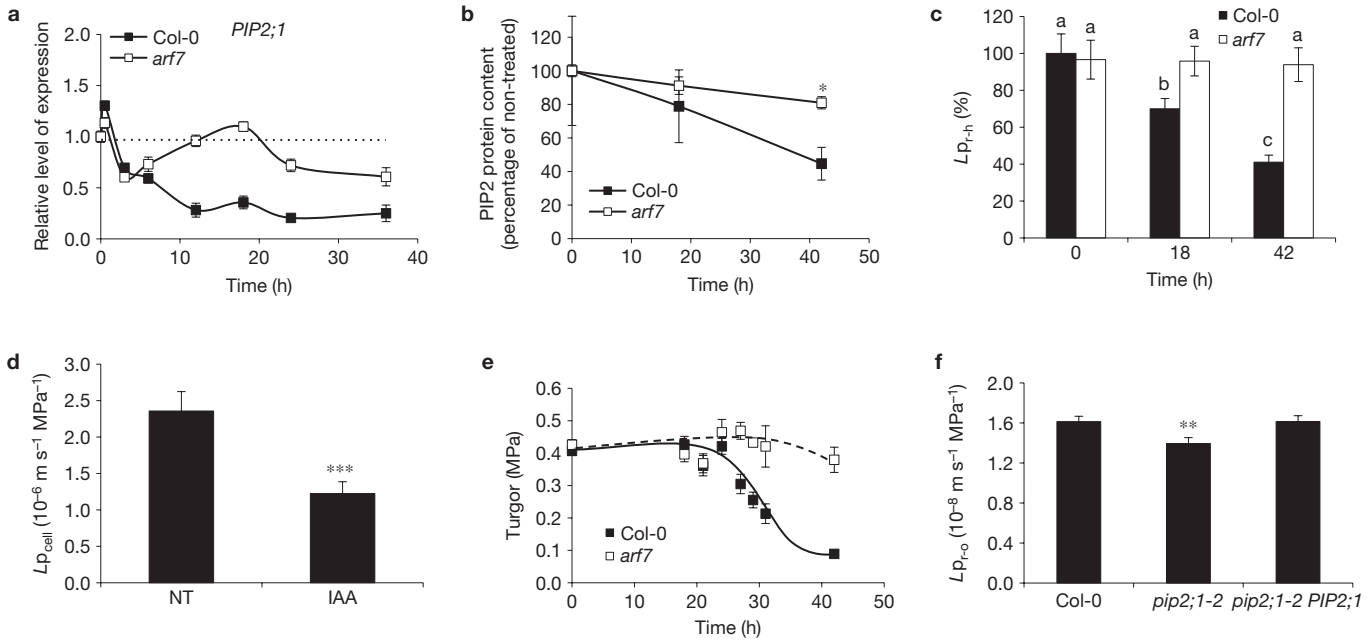

Figure 2 Auxin reduces aquaporin accumulation and hydraulic conductivity. (**a**) Auxin-dependent repression of one of the most highly expressed root isoforms, *PIP2;1*, is *ARF7* dependent. (**b**) The protein content was determined by ELISA with a anti-PIP2 antibody that recognizes PIP2;1, PIP2;2 and PIP2;3. Roots were collected after treatment with 1 μM IAA for the indicated time on wild-type (Col-0) and *arf7* mutant plants. Values are indicated as a percentage of the untreated control from three independent plant cultures. (**c**) Lp_{r-h} was measured after 1 μM IAA treatment for 18 and 42 h on Col-0 and the *arf7* mutant. Values are indicated as a percentage of the untreated Col-0 ($9 < n < 29$). (**d**) Lp_{cell} of Col-0 roots was measured after treatment for 18 h with 1 μM IAA ($n = 22$) and compared with the Lp_{cell} of non-treated (NT) roots. (**e**) Cortical cell turgor was reduced on auxin treatment in Col-0 but not in the *arf7* mutant. (**f**) Lp_{r-o} was determined in the wild type (Col-0), *pip2;1-2* mutant and complemented *pip2;1-2* mutant (*pip2;1-2 PIP2;1*). Data shown are mean value ± s.e.m. with $n = 21$, 18 and 22 assessed from two independent plant cultures. The asterisks indicate a significant difference from the corresponding control experiment by Student's *t*-test ($^{*}P < 0.05$; $^{**}P < 0.01$; $^{***}P < 0.001$). The letters indicate independent groups according to one-way analysis of variance test (**c**).

spatial and temporal control of water exchanges between the stele, LRP and overlaying cells.

Modelling suggests that distinct spatial domains of aquaporin expression are required during LRE

To gain further understanding of the biomechanics of LRE and how this process is affected by the presence of auxin and aquaporins, we developed a mathematical model, which simulates water movement between stele, LRP and overlaying tissues. We considered the tissue scale and modelled the primordium and overlaying tissue as distinct fluid-like compartments, lumping the effects of cell-wall extension and cell-to-cell reorganization into the properties of the boundaries (Fig. 4a).

In the model (see Supplementary Information), we assumed that emergence is driven by increasing osmotic pressure within dividing primordium cells, drawing water into the LRP and resulting in a build-up in turgor pressure. This pressure increases the stress in the LRP boundary, which eventually yields and extends, enabling the LRP to force through the overlaying tissues. The predicted emergence time depends on the material properties of the LRP boundary (characterized by extensibility and yield), initial tissue configuration (considered to be a stage I primordium) and magnitude of water fluxes. The presence of aquaporins increases the boundary permeability whereas auxin accumulation leads to its decrease. Thus, the model enabled us to deduce how LRE is affected by the aquaporin distribution and its regulation by auxin.

The model can be described using differential equations with appropriate initial conditions and kinetic parameters estimated from experiments (see Supplementary Information). We adjusted the rate of increase of the primordium's osmotic pressure so that LRE took 28 h in wild-type plants (Fig. 4b). The model predicted the hydrostatic pressures in the primordium and overlaying tissue, and the direction of the water fluxes through each boundary (shown by arrows in Fig. 4a). The model also revealed how the boundary permeabilities (k_1 to k_4) affect the emergence time (Fig. 4c,d); we obtained a significant influence provided the yield stress of the primordium's boundary is small, suggesting significant cell-wall remodelling as reported previously[5,34]. The model predicted that increasing k_2 or k_4 inhibits emergence by facilitating water movement into overlaying tissues (Fig. 4c,d). In contrast, increasing k_1 promotes emergence by facilitating water inflow into the primordium whereas increasing k_3 has an opposite effect on emergence by favouring water outflow towards the stele (Fig. 4c,d).

Owing to the direction of the water fluxes, the model predicted that, by reducing aquaporin activity in the overlaying tissue (reducing permeability k_2), auxin promotes emergence. However, auxin also inhibits emergence by reducing aquaporin activity in the primordium (reducing permeability k_1). To understand these opposing effects, we removed the influence of auxin from the model (making k_1 and k_2 constant); with appropriate parameter values, we found emergence to be delayed by 8.7 h, indicating that, indeed, auxin has an accelerating effect on LRE. Thus, the model exemplifies how spatial

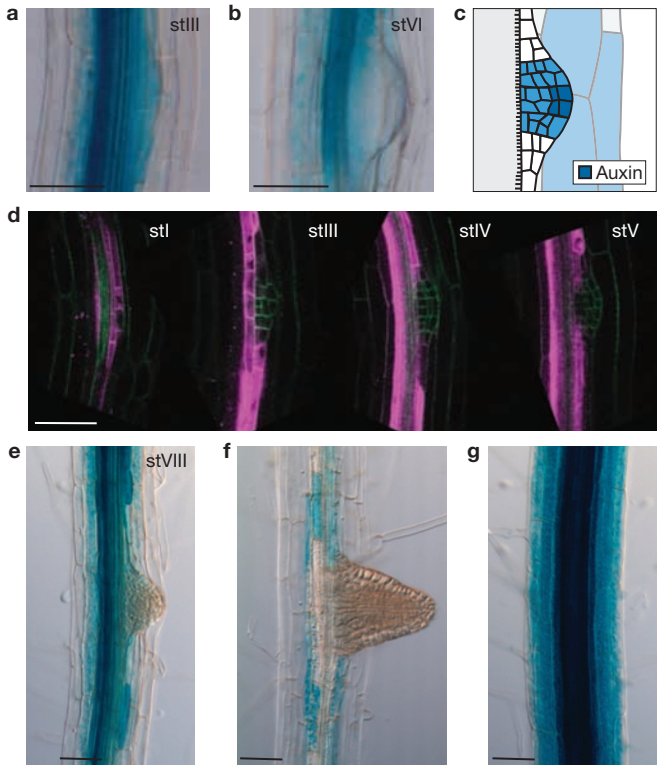

Figure 3 *PIP2;1* expression oppositely mirrors auxin accumulation during lateral root formation. (**a**,**b**) *PIP2;1* expression determined with a transcriptional *proPIP2;1:GUS* fusion. (**c**) Schematic drawing showing auxin accumulation in the LRP and the overlaying tissue as reported by the auxin responsive promoter DR5 (refs 5,21). (**d**) *PIP2;1* expression determined with a translational *proPIP2;1:PIP2;1–mCHERRY* fusion (magenta). Cell shapes are indicated by the plasma-membrane-localized marker (green) encoded by *proUBQ:YFP–NPSN12*. (**e**–**g**) Auxin controls the *PIP2;1* expression pattern: untreated seven-day-old plants (**e**), plants treated with 1 μM IAA for 48 h (**f**) and plants treated with 10 μM PCIB for 24 h (**g**). The lateral root developmental stages are indicated by roman numbers as described previously[20]. Scale bars, 50 μm.

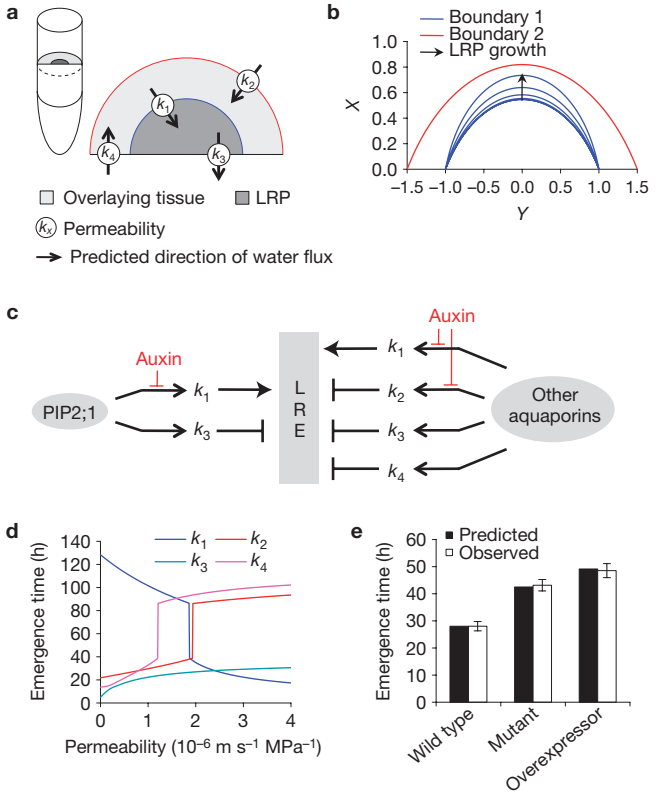

Figure 4 Mathematical model of LRE. (**a**) Two-dimensional tissue-scale model of LRE representing the cross-section of an LRP (dark grey) protruding into the outer tissue (light grey). The arrows show the predicted direction of the water fluxes between compartments; the magnitude of each water flux depends on the boundary's permeability (k_1 to k_4) and the difference in hydrostatic pressure and osmotic potential. (**b**) Simulation of the wild-type LRP emerging through the overlaying tissue. (**c**) Diagram summarizing how auxin and aquaporins affect the permeabilities, and how these in turn affect the predicted emergence time. (**d**) The influence of the permeability values on the predicted emergence time. (**e**) The predicted and observed emergence times in the wild type, the *pip2;1* mutant and the *PIP2;1* overexpressor (see Supplementary Information for choice of parameter values). Data shown are mean value ± s.e.m., and $n = 20$.

and temporal control of auxin-dependent cell hydraulic conductivity could be critical during LRE.

We next used the model to investigate the importance of the cell-specific and dynamic *PIP2;1* distribution. We first simulated LRE with *PIP2;1* expression being ectopic and independent of auxin. This PIP2;1 distribution facilitated water fluxes into the overlaying tissue, resulting in this tissue providing a greater resistance to primordium expansion and therefore delaying LRE by >20 h (Fig. 4e). We then considered a loss-of-function mutant, *pip2;1*, by reducing permeabilities k_1 and k_3 and removing auxin's influence on k_1. Reducing k_1 (inhibiting LRE by reducing fluxes into the primordium) dominates over the influence of reducing k_3 (promoting LRE by reducing fluxes out of the primordium), so that LRE should again occur later than in the wild type (emergence time: 42.5 h), owing to reduced water fluxes from the overlaying tissue to the primordium (Fig. 4e). Thus, the model shows how the spatial distribution of PIP2;1 promotes LRE.

Phenotypes of PIP2;1-knockout and -overexpressing lines validate model predictions

To test model predictions, we studied transgenic lines expressing *PIP2;1* under the control of the strong, constitutive double 35S promoter (*d35S:PIP2;1*). *PIP2;1* overexpression led to a concomitant increase in PIP2 abundance and $Lp_{r\text{-}h}$ (+47 − 63%—Supplementary Fig. S4a,b). In addition, the transgenic lines showed a complete insensitivity of $Lp_{r\text{-}h}$ to auxin inhibition (Supplementary Fig. S4c). Next, wild-type and transgenic roots were given a gravitropic stimulus and LRP were counted and staged at 18 and 42 h pgi (Fig. 5a,b). Wild-type (Col-0) plants accumulated stage I and II LRP 18 h pgi and stage VII and VIII 42 h pgi, respectively (Fig. 5a). Lateral root initiation and first divisions were not affected in *d35S:PIP2;1*, but showed an accumulation of stage II–VIII LRP 42 h pgi (Fig. 5b). This result indicates impaired LRE after aquaporin overexpression, as predicted in the mathematical model (Fig. 4e).

In parallel, we analysed the effects of two independent loss-of-function alleles in *PIP2;1*. Lateral root initiation and first divisions were not affected in the *pip2;1-1* and *pip2;1-2* mutants, but LRE was delayed at 42 h pgi (Fig. 5a,c,d). Mutant *pip2;1-1* and *pip2;1-2* plants transformed with a 4.6-kilobase (kb) genomic fragment containing the full *PIP2;1* gene or a *proPIP2;1:PIP2;1–mCHERRY* construct exhibited a wild-type LRE phenotype on lateral root induction (Fig. 5e,f and

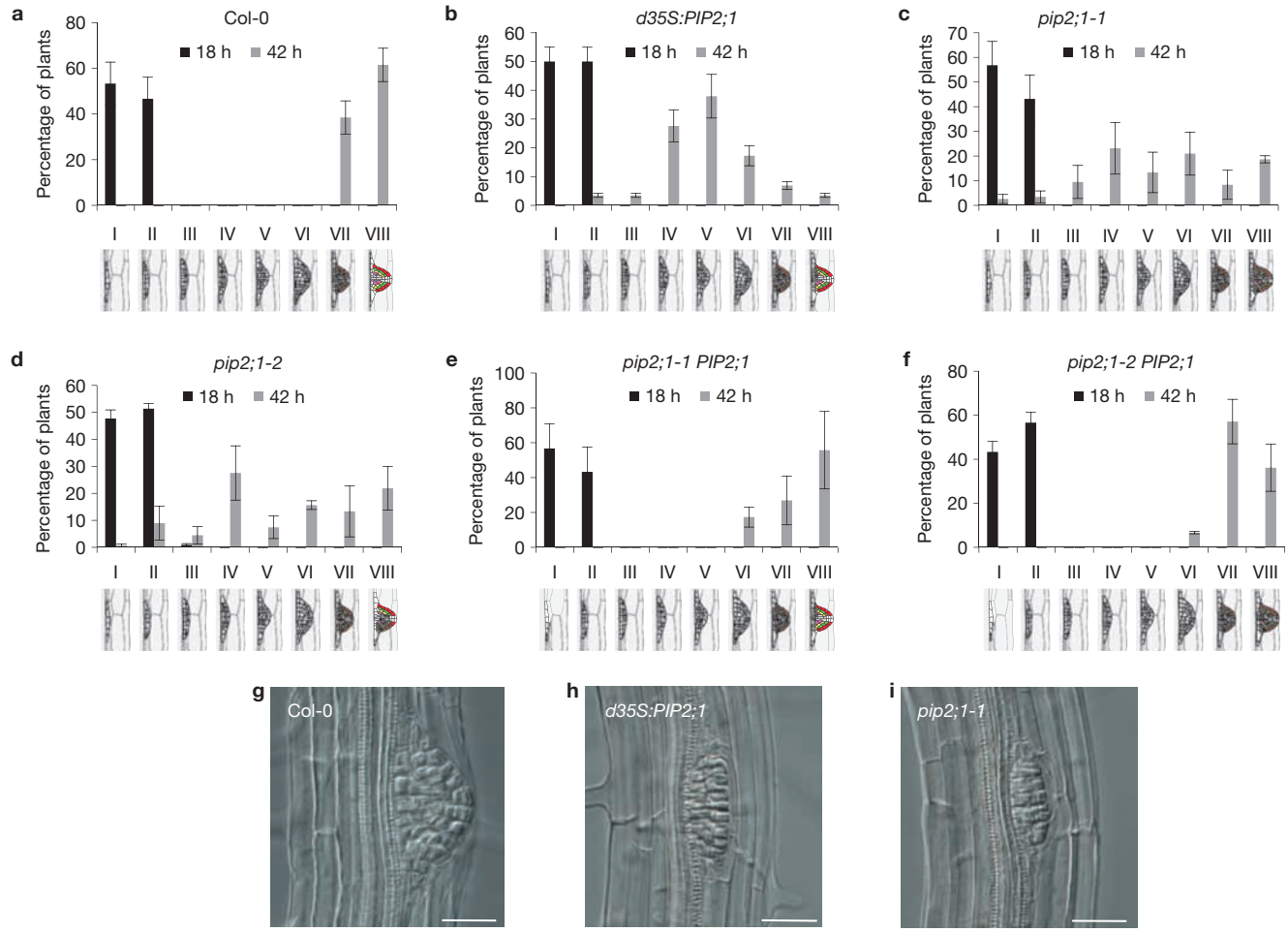

Figure 5 LRE is delayed in the *pip2;1* mutant and the *PIP2;1* overexpressor. (**a**–**f**) LRE phenotyping was achieved by synchronizing lateral root formation with a gravistimulus. Primordia were grouped according to developmental stages as defined previously[20] 18 h pgi (black bars) and 42 h pgi (grey bars). (**a**) Wild-type (Col-0) plants showed accumulation of stage I and II primordium 18 h pgi and accumulation of stage VII and VIII 42 h pgi. (**b**) The *PIP2;1*-overexpression line (*d35S:PIP2;1*) showed similar stages of lateral root formation at 18 h pgi when compared with the wild type, thereby suggesting that early stages of lateral root development were not affected. However, most LRP accumulated at stage IV–VI at 42 h pgi, indicating an emergence defect. (**c**,**d**) LRE is delayed in loss-of-function *pip2;1* mutants. The *pip2;1-1* and *pip2;1-2* mutants showed similar stages of lateral root formation at 18 h pgi when compared to the wild type, thereby suggesting that early stages of lateral root development were not affected. However, only a small amount of LRP reached stages VII and VIII at 42 h pgi in the mutant, indicating an emergence defect. (**e**–**f**) Complementation of both the *pip2;1-1* and *pip2;1-2* mutant alleles with the *PIP2;1* genomic sequence resulted in restoration of the wild-type LRE phenotype. (**g**–**i**) Differential interference contrast imaging at 42 h pgi showed abnormal LRP in the *d35S:PIP2;1* line and the *pip2;1-1* mutant when compared with the dome-shaped wild-type primordium. Data shown are mean value ± s.e.m. and $n = 20$ (**a**–**f**). Scale bars, 25 μm.

Supplementary Fig. S5), demonstrating that the LRE defect was due to disruption of the *PIP2;1* gene. In addition, the LRP shape of both PIP2;1-knockout and overexpressing lines was altered when compared with the wild type (Fig. 5g–i). Whereas wild-type LRP form a dome-shape, mutant LRP were flattened and failed to protrude into overlaying tissues (Fig. 5h,i). Hence, loss of *PIP2;1* function resulted in defective LRE, consistent with the predictions made by the model (Fig. 4e).

DISCUSSION

The hormone auxin represents a key regulator of lateral root development[3]. Previous work has demonstrated that specialized efflux and influx transport proteins cause auxin to accumulate at the apex of new LRP and in overlaying cells, respectively[5,21]. Auxin triggers cell-wall remodelling gene expression in the overlaying cells[34], thereby facilitating primordium emergence through the outer tissues[5]. It was proposed that LRE and concomitant physical modification of the outer tissues must be tightly co-regulated. Here, we demonstrate that auxin also regulates tissue hydraulics to promote LRE.

Auxin regulates root tissue hydraulics by coordinating the repression of aquaporin gene expression in the LRP and overlaying tissues. Application of exogenous auxin and mutant analysis revealed crucial features of hormone action, namely its marked effects on root hydraulics at both the whole-root ($Lp_{r\text{-}o}$ and $Lp_{r\text{-}h}$) and single-cell (Lp_{cell}) levels; dependency on auxin response factor ARF7; and the similar phenotypic defects in LRP shape and LRE kinetics in *arf7* and *pip2;1* mutants (Fig. 5 and Supplementary Fig. S6a–d). These features indicate that regulation of the tissue distribution of aquaporins by auxin fine-tunes the spatial and temporal control of root tissue hydraulics. Although these hydraulic effects can lead to a dynamic decrease in overlaying cells' turgor, as exemplified in the model, turgor measurements in

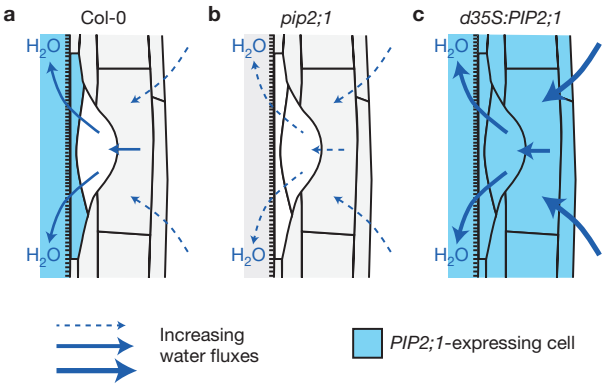

Figure 6 Diagram illustrating the regulation of LRE by PIP2;1. (**a**) Optimal LRE requires water transport into the overlaying tissue to be repressed as a result of auxin accumulation. (**b**) In the *pip2;1* loss-of-function mutant, water transport within the primordium and towards the vasculature is altered, resulting in a reduced LRE rate. (**c**) In the *PIP2;1* gain-of-function mutant, water transport is globally increased, notably in the outer tissue where water transport is normally repressed by auxin. As a result, LRE is delayed.

auxin-treated roots (Fig. 2e) suggested that auxin may also exert more direct effects on steady-state cell turgor. The overall result points to the pivotal role of auxin in controlling the biomechanics of LRE, whereby this hormone affects tissue plasticity (through cell-wall enzymes), water supply (through aquaporins) and turgor maintenance to promote the emergence of developing LRP through overlaying tissues.

Plant roots express numerous aquaporin isoforms[22,23]. The present work focused on the regulation and function of PIP2;1, one of most highly expressed PIPs. Using a high-resolution lateral root synchronization procedure, we showed that disrupting *PIP2;1* gene function impacts lateral root morphogenesis, causing the normal dome-like shape to become flattened, and significantly delays the time taken for the new organ to emerge. *PIP2;1* belongs to a subset of *PIP2* genes (*PIP2;1*, *PIP2;4* and *PIP2;6*) whose messenger RNA abundance exhibits a transient induction before they are repressed along with most other aquaporin genes expressed during lateral root development (Fig. 1c). In only two cases (*PIP2;5* and *PIP2;8*) are *PIP2* transcript levels enhanced throughout lateral root development (Fig. 1d). The spatial pattern of *PIP2;8* expression revealed that it was specifically upregulated at the base of LRP and in the underlying stele (Supplementary Fig. S3). Monitoring the expression patterns and functional importance of every other aquaporin gene family member during lateral root development would provide more insight into their potentially contrasting roles during organ emergence. Preliminary characterization of knockout mutations in other *PIP2* genes has revealed that, similarly to *pip2;1*, they cause a delay in LRE (Supplementary Fig. S6c,e–g). As PIP2;2 is another major root aquaporin with an expression profile similar to PIP2;1 during LRE (Fig. 1c), we also examined the combined loss-of-function mutations in *PIP2;1* and *PIP2;2*. The double mutant showed a delay in LRE similar to the *pip2;1* mutant (Supplementary Fig. S6c,h) consistent with PIP2;1 being the main aquaporin in root tissues. Thus, the present study opens the way to a detailed genetic dissection of the hydraulic control of tissue growth involving other PIP isoforms, at a level of resolution not previously achieved in a plant system.

To probe the tissue-scale regulatory mechanism(s) for how auxin control of aquaporin activity affects LRE, we developed a mathematical model of the root cross-section that describes water fluxes and primordium expansion. Our results suggested that optimal LRE requires water transport into the overlaying tissue to be repressed as a result of auxin accumulation, whereas aquaporins would promote water transfer from the overlaying cells into the primordium (Figs 4a,c and 6a) . These opposing effects on LRE have therefore to be precisely tuned in time and space to explain an overall beneficial effect of auxin and aquaporin activation and repression on LRE. Simulations help provide insight into this integrated process and predict that adding ectopic constitutive *PIP2;1* expression, or removing either tissue-specific *PIP2;1* distribution or auxin inhibition of aquaporins resulted in a reduced emergence rate (Fig. 4), in agreement with experimental observations (Fig. 5). Thus, the model revealed that, in the *pip2;1* loss-of-function mutant, LRE was delayed owing to reduced water transport from the overlaying tissue into the primordium (the k_1 pathway; Fig. 4a and Fig. 6b), whereas in roots of *PIP2;1*-overexpressing plants, it was caused by an increased water supply to the overlaying cells (the k_2 and k_4 pathways; Figs 4a and 6c).

Although the modelling approach allowed us to explain counter-intuitive behaviour, in particular when considering similar LRE phenotypes caused by gain- or loss-of-function of *PIP2*, the phenotypic characterization of additional aquaporin genotypes will help refine this approach and estimates of crucial parameter values. By focusing on the tissue scale, the model also provides a building block in developing future models, which should incorporate the cell scale and three-dimensionality, which we believe will assist in understanding the interplay between the regulation of the water fluxes investigated here, and the remodelling of cell walls, to provide an optimal separation of the overlaying cells. □

METHODS

Methods and any associated references are available in the online version of the paper.

Note: Supplementary Information is available in the online version of the paper

ACKNOWLEDGEMENTS

This work was supported by a Marie Curie Intra-European Fellowship within the 7th European Community Framework Programme PIEF-GA-2008-220506 (B.P.) and by a Grand Federative Project (*Rhizopolis*) of the Agropolis Fondation (Montpellier, France) to C.M. We are indebted to H. Scherb (Helmholtz Zentrum München) for his help with statistical analyses. L.R.B., U.V., M.L., D.M.W., J.R.K., O.E.J. and M.J.B. acknowledge the support of the Biotechnology and Biological Sciences Research Council (BBSRC) and Engineering and Physical Sciences Research Council (EPSRC) funding to the Centre for Plant Integrative Biology (CPIB), BBSRC responsive mode grant support to U.V., L.R.B. and M.J.B. and the BBSRC Professorial Research Fellowship funding to D.M.W. and M.J.B. A.R.S. and O.D.I. acknowledge the support of the Deutsche Forschungsgemeinschaft priority programme SPP1108 (SCHA 454/8).

AUTHOR CONTRIBUTIONS

B.P., G.L., J.Z., U.V., O.P., D-T.L., O.D.I., I.C., M.L., D.M.W., L.L. and P.N. performed experimental work; B.P., G.L., J.Z., L.R.B., J.R.K., O.E.J., A.R.S., C.M. and M.J.B. performed data analysis; B.P., L.R.B., J.R.K., O.E.J., A.R.S., C.M. and M.J.B. oversaw project planning; B.P., L.R.B., A.R.S., C.M. and M.J.B. wrote the paper.

COMPETING FINANCIAL INTERESTS

The authors declare no competing financial interests.

Published online at www.nature.com/doifinder/10.1038/ncb2573
Reprints and permissions information is available online at www.nature.com/reprints

1. Casimiro, I. *et al.* Dissecting *Arabidopsis* lateral root development. *Trends Plant Sci.* **8,** 165–71 (2003).
2. Péret, B., Larrieu, A. & Bennett, M. J. Lateral root emergence: a difficult birth. *J. Exp. Bot.* **60,** 3637–43 (2009).
3. Péret, B. *et al. Arabidopsis* lateral root development: an emerging story. *Trends Plant Sci.* **14,** 399–408 (2009).
4. Overvoorde, P., Fukaki, H. & Beeckman, T. Auxin control of root development. *Cold Spring Harb. Perspect. Biol.* **2,** a001537 (2010).
5. Swarup, K. *et al.* The auxin influx carrier LAX3 promotes lateral root emergence. *Nat. Cell Biol.* **10,** 946–54 (2008).
6. Cosgrove, D. J. Water uptake by growing cells: an assessment of the controlling roles of wall relaxation, solute uptake, and hydraulic conductance. *Int. J. Plant Sci.* **154,** 10–21 (1993).
7. Boyer, J. S. & Silk, W. K. Hydraulics of plant growth. *Funct. Plant Biol.* **31,** 761–773 (2004).
8. Ehlert, C., Maurel, C., Tardieu, F. & Simonneau, T. Aquaporin-mediated reduction in maize root hydraulic conductivity impacts cell turgor and leaf elongation even without changing transpiration. *Plant Physiol.* **150,** 1093–104 (2009).
9. Fricke, W. Biophysical limitation of cell elongation in cereal leaves. *Ann. Bot.* **90,** 157–67 (2002).
10. Hukin, D., Doering-Saad, C., Thomas, C. R. & Pritchard, J. Sensitivity of cell hydraulic conductivity to mercury is coincident with symplasmic isolation and expression of plasmalemma aquaporin genes in growing maize roots. *Planta* **215,** 1047–56 (2002).
11. Oparka, K. J., Prior, D. A. M. & Wright, K. M. Symplastic communication between primary and developing lateral roots of *Arabidopsis thaliana*. *J. Exp. Bot.* **46,** 187–197 (1995).
12. Gomes, D. *et al.* Aquaporins are multifunctional water and solute transporters highly divergent in living organisms. *Biochim. Biophys. Acta* **1788,** 1213–28 (2009).
13. Danielson, J. A. & Johanson, U. Phylogeny of major intrinsic proteins. *Adv. Exp. Med. Biol.* **679,** 19–31 (2010).
14. Kaldenhoff, R. *et al.* Aquaporins and plant water balance. *Plant Cell Environ.* **31,** 658–66 (2008).
15. Maurel, C., Verdoucq, L., Luu, D. T. & Santoni, V. Plant aquaporins: membrane channels with multiple integrated functions. *Annu. Rev. Plant Biol.* **59,** 595–624 (2008).
16. Ditengou, F. A. *et al.* Mechanical induction of lateral root initiation in *Arabidopsis thaliana*. *Proc. Natl Acad. Sci. USA* **105,** 18818–23 (2008).
17. Laskowski, M. *et al.* Root system architecture from coupling cell shape to auxin transport. *PLoS Biol.* **6,** 2721–2735 (2008).
18. Lucas, M., Godin, C., Jay-Allemand, C. & Laplaze, L. Auxin fluxes in the root apex co-regulate gravitropism and lateral root initiation. *J. Exp. Bot.* **59,** 55–66 (2008).
19. Richter, G. L., Monshausen, G. B., Krol, A. & Gilroy, S. Mechanical stimuli modulate lateral root organogenesis. *Plant Physiol.* **151,** 1855–66 (2009).
20. Malamy, J. E. & Benfey, P. N. Organization and cell differentiation in lateral roots of *Arabidopsis thaliana*. *Development* **124,** 33–44 (1997).
21. Benková, E. *et al.* Local, efflux-dependent auxin gradients as a common module for plant organ formation. *Cell* **115,** 591–602 (2003).
22. Alexandersson, E. *et al.* Whole gene family expression and drought stress regulation of aquaporins. *Plant Mol. Biol.* **59,** 469–84 (2005).
23. Monneuse, J. M. *et al.* Towards the profiling of the *Arabidopsis thaliana* plasma membrane transportome by targeted proteomics. *Proteomics* **11,** 1789–97 (2011).
24. Calderon-Villalobos, L. I., Tan, X., Zheng, N. & Estelle, M. Auxin perception–structural insights. *Cold Spring Harb. Perspect. Biol.* **2,** a005546 (2010).
25. Okushima, Y. *et al.* Functional genomic analysis of the AUXIN RESPONSE FACTOR gene family members in *Arabidopsis thaliana*: unique and overlapping functions of ARF7 and ARF19. *Plant Cell* **17,** 444–63 (2005).
26. Okushima, Y., Fukaki, H., Onoda, M., Theologis, A. & Tasaka, M. ARF7 and ARF19 regulate lateral root formation via direct activation of LBD/ASL genes in *Arabidopsis*. *Plant Cell* **19,** 118–30 (2007).
27. Wilmoth, J. C. *et al.* NPH4/ARF7 and ARF19 promote leaf expansion and auxin-induced lateral root formation. *Plant J.* **43,** 118–30 (2005).
28. De Smet, I. *et al.* Bimodular auxin response controls organogenesis in *Arabidopsis*. *Proc. Natl Acad. Sci. USA* **107,** 2705–10 (2010).
29. Santoni, V., Vinh, J., Pflieger, D., Sommerer, N. & Maurel, C. A proteomic study reveals novel insights into the diversity of aquaporin forms expressed in the plasma membrane of plant roots. *Biochem J.* **373,** 289–96 (2003).
30. Javot, H. *et al.* Role of a single aquaporin isoform in root water uptake. *Plant Cell* **15,** 509–22 (2003).
31. Boursiac, Y. *et al.* Stimulus-induced downregulation of root water transport involves reactive oxygen species-activated cell signalling and plasma membrane intrinsic protein internalization. *Plant J.* **56,** 207–18 (2008).
32. Kazama, H. & Katsumi, M. The role of the osmotic potential of the cell in auxin-induced cell elongation. *Plant Cell Physiol.* **19,** 1145 (1978).
33. Da Ines, O. *et al.* Kinetic analyses of plant water relocation using deuterium as tracer-reduced water flux of *Arabidopsis* pip2 aquaporin knockout mutants. *Plant Biol. (Stuttg)* **12** (Suppl. 1), 129–39 (2010).
34. Laskowski, M., Biller, S., Stanley, K., Kajstura, T. & Prusty, R. Expression profiling of auxin-treated *Arabidopsis* roots: toward a molecular analysis of lateral root emergence. *Plant Cell Physiol.* **47,** 788–92 (2006).

METHODS

Growth conditions and plant material. Wild-type Columbia (Col-0), mutants (*arf7-1*[25], *pip2;1* and *pip2;1 pip2;2*) and reporter lines were grown on vertical 1/2 Murashige–Skoog (MS) plates at 23 °C under continuous light (150 μmol m^{-2} s^{-1}). *pip2;1-1* is derived from the AMAZE collection[35] and the En-transposon is inserted after the 69th nucleotide of the second exon; *pip2;1-2*, *pip2;2-3* and *pip2;2-4* have been described previously[33]. *pip2;4-1* (SM_3_20853; ref. 36) and *pip2;6-3* (SALK_ 092140; ref. 37) were obtained from the Nottingham Arabidopsis Stock Centre[38] and verified by genotyping and RT–PCR. The *pip2;1 pip2;2* double mutant was generated by crossing *pip2;1-2* and *pip2;2-3*. *proPIP2;1:GUS* lines have been described previously[33]. A fragment comprising 2,526 base pairs upstream of the start codon of *PIP2;8* (At2g16850) was cloned into pBGWFS7 to generate transcriptional *proPIP2;8:GUS* fusions. For lateral root phenotypical analysis, lateral root induction was performed on three-day-old seedlings by rotating the plates at 90°. For expression analysis, six-day-old plants were transferred on vertical 1/2 MS plates supplemented with 1 μM IAA or 10 μM PCIB for the indicated time. For root water transport measurements and ELISA assays, plants were germinated and grown on plates for 10 days before transfer to hydroponic culture, as previously described[30]. Plants were further grown for 10–20 days, in a growth chamber at 70% relative humidity with cycles of 16 h of light (250 μmol m^{-2} s^{-1}) at 22 °C and 8 h of dark at 21 °C.

Nucleic-acid manipulations and constructs. For overexpression of *A. thaliana* PIP2;1, the complementary DNA of PIP2;1 was placed under the control of a double enhanced CaMV 35S promoter and transferred into plants through *Agrobacterium* by floral dipping[39] using a pGreen179 binary transformation vector. Three plant lines that showed the highest expression of the transgene were selected among 200 transformed lines by western blot analyses on leaf extract using an anti-PIP2 antibody[29] (see below). Plants co-expressing the *PIP2;1–mCHERRY* construct under the control of 1.5 kb of genomic sequences upstream of the *PIP2;1* start codon, and the *YFP–AtNPSN12* construct under the control of a promoter of ubiquitin 10 gene[40] were obtained by crossing the plants that individually express the constructs. *At* NPSN12 is a SNARE protein, which has been localized in the plasma membrane[40].

Mutant complementation. A 4.6 kb genomic *PIP2;1* fragment was amplified by PCR using primers 5′-ATTTGTCCTTTCCGGTACAAT-3′ (forward) and 5′-ACTCTCAATCCTCAGCCAAGT-3′ (reverse) and cloned into pDONR221 vector, verified by sequencing and subsequently cloned into pBGW and transformed by floral dipping[39] into the two *pip2;1* mutant alleles. Homozygous, complemented plants with single insertion were confirmed on the basis of antibiotic (phosphinotricine) resistance and further confirmed by RT–PCR.

qRT–PCR. Total RNA was extracted from roots using a Qiagen RNeasy plant mini kit with on-column DNAse treatment (RNAse free DNAse set, Qiagen). Poly(dT) cDNA was prepared from 2 μg total RNA using the Transcriptor first-strand cDNA synthesis kit (Roche). qPCR was performed using SYBR Green Sensimix (Quantace) on Roche LightCycler 480 apparatus. PCR was carried out in 384-well optical reaction plates heated for 1 min to 95 °C, followed by 40 cycles of denaturation for 5 s at 95 °C, annealing for 8 s at 62 °C and extension for 30 s at 72 °C. Target quantifications were performed with the specific primer pairs described in Supplementary Fig. S7. Expression levels were normalized to the ubiquitin-associated gene *UBA* (At1g04850) using the following primers *UBA* forward 5′-agtggagaggctgcagaaga-3′ and *UBA* reverse 5′-ctcgggtagcacgagcttta-3′. All qRT–PCR experiments were performed in triplicate and the values represent means ± s.e.m.

Hydraulic conductivity measurement. Measurements of root hydrostatic hydraulic conductivity (Lp_{r-h}) and root osmotic hydraulic conductivity (Lp_{r-o}) were performed as described previously[30,41]. Pressure probe measurements in root cortical cells and calculation of cell hydraulic conductivity were made as previously described[30].

Immunodetections. Serial twofold dilutions in a carbonate buffer (30 mM Na_2CO_3, 60 mM $NaHCO_3$, at pH 9.5) of 0.5 μg of membrane extracts were loaded in triplicate on immunoplates (Maxisorp). The ELISA assay was performed as previously described[42] using a 1:2,000 dilution of an anti-PIP2 antibody raised against a 17-amino-acid carboxy-terminal peptide of *At* PIP2;1 (ref. 29). Western blot analysis was performed using classical procedures[29] and the same anti-PIP2 antibody.

Histochemical analysis and microscopy. GUS staining was done as previously described[43]. Plants were cleared for 24 h in 1 M chloral hydrate and 33% glycerol. Seedlings were mounted in 50% glycerol and observed with a Leica DMRB microscope. For confocal microscopy, images were captured with an inverted confocal laser-scanning microscope (Inverse 1 Axiovert 200M Zeiss/LSM 510 META Confocal) with a 63× oil-immersion objective. The emitted fluorescence signal was captured by alternately switching the 488 nm and 543 nm excitation lines. Lateral roots were imaged as 1 μm step *z* series.

Mathematical modelling. Full details of the model formulation and predictions are provided in the Supplementary Information. Details of the modelling are available in Supplementary Note S1 and Matlab code is available in Supplementary Data S1. Simulations were performed in Matlab and the numerical code can be downloaded from www.cpib.ac.uk/tools-resources/models.

35. Wisman, E., Cardon, G. H., Fransz, P. & Saedler, H. The behaviour of the autonomous maize transposable element En/Spm in *Arabidopsis thaliana* allows efficient mutagenesis. *Plant Mol. Biol.* **37,** 989–99 (1998).
36. Tissier, A. F. *et al.* Multiple independent defective suppressor-mutator transposon insertions in *Arabidopsis*: a tool for functional genomics. *Plant Cell* **11,** 1841–52 (1999).
37. Alonso, J. M. *et al.* Genome-wide insertional mutagenesis of *Arabidopsis thaliana*. *Science* **301,** 653–657 (2003).
38. Scholl, R. L., May, S. T. & Ware, D. H. Seed and molecular resources for *Arabidopsis*. *Plant Physiol.* **124,** 1477–1480 (2000).
39. Clough, S. J. & Bent, A. F. Floral dip: a simplified method for Agrobacterium-mediated transformation of *Arabidopsis thaliana*. *Plant J.* **16,** 735–43 (1998).
40. Geldner, N. *et al.* Rapid, combinatorial analysis of membrane compartments in intact plants with a multicolor marker set. *Plant J.* **59,** 169–78 (2009).
41. Postaire, O. *et al.* A PIP1 aquaporin contributes to hydrostatic pressure-induced water transport in both the root and rosette of *Arabidopsis*. *Plant Physiol.* **152,** 1418–30 (2010).
42. Boursiac, Y. *et al.* Early effects of salinity on water transport in *Arabidopsis* roots. Molecular and cellular features of aquaporin expression. *Plant Physiol.* **139,** 790–805 (2005).
43. Péret, B. *et al.* Auxin influx activity is associated with Frankia infection during actinorhizal nodule formation in *Casuarina glauca*. *Plant Physiol.* **144,** 1852–62 (2007).

DOI: 10.1038/ncb2573

nature cell biology

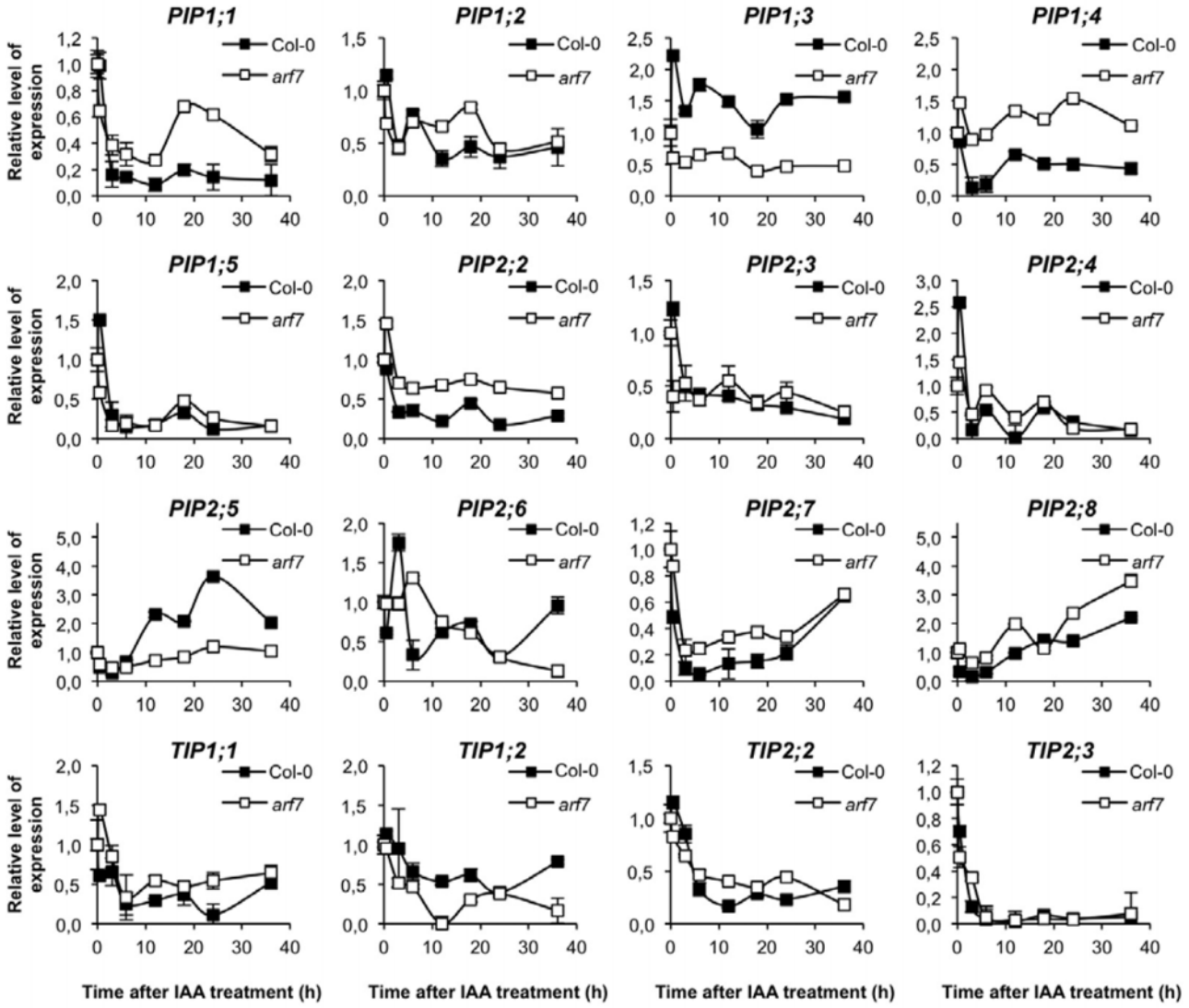

Figure S1 Expression analysis of the major aquaporin genes. Average relative level of expression and sem values of aquaporin genes (*PIP1;1*, *PIP1;2*, *PIP1;3*, *PIP1;4*, *PIP1;5*, *PIP2;2*, *PIP2;3*, *PIP2;4*, *PIP2;6*, *PIP2;7*, *TIP1;1*, *TIP1;2*, *TIP2;2*, and *TIP2;3*) upon 1 μM IAA treatment in the wild type (WT) and *arf7* mutant backgrounds. Time is indicated in hours.

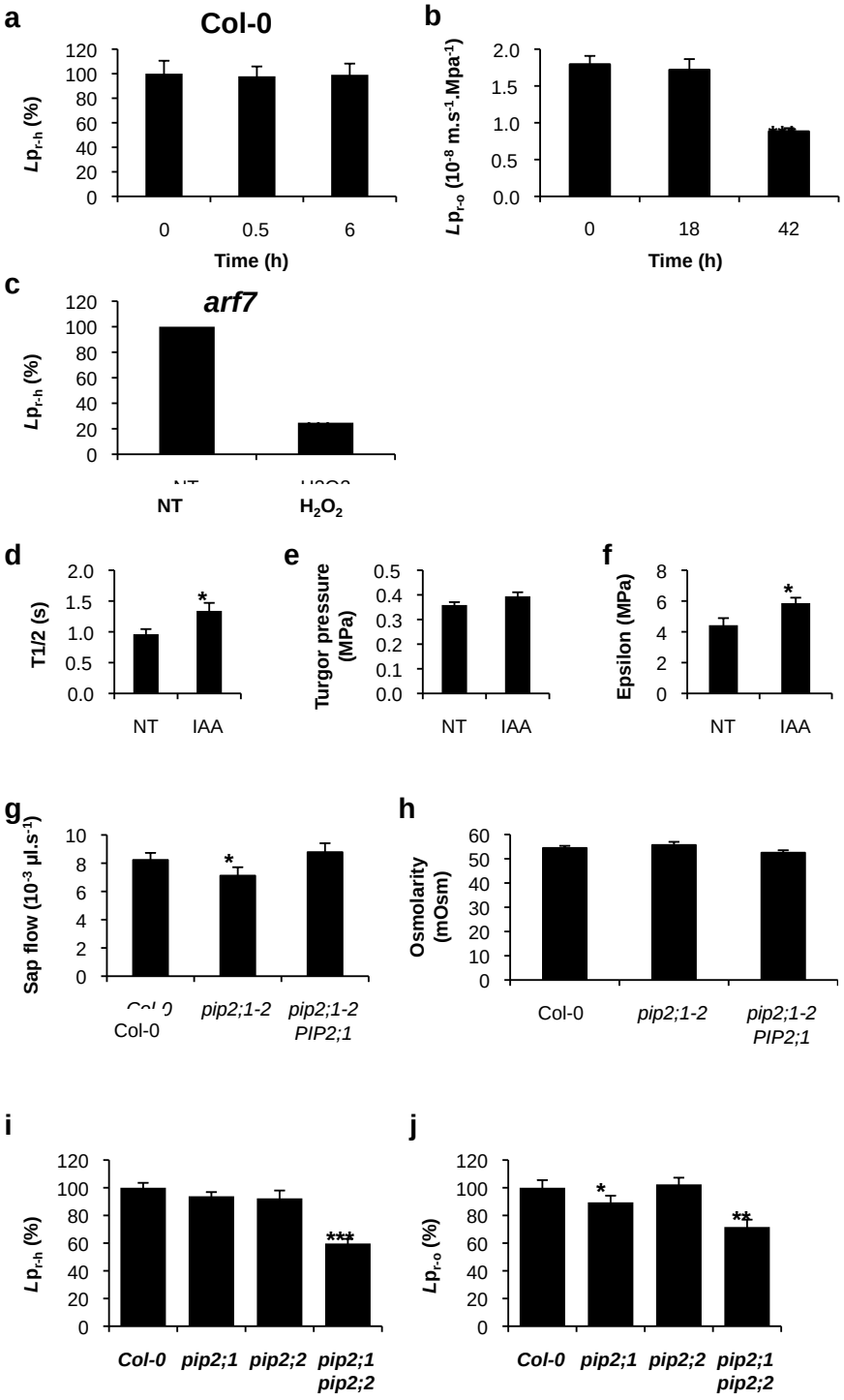

Figure S2 Supplementary root hydraulic conductivity measurements. (**a**) Short time 1 µM IAA treatment did not affect hydrostatic root hydraulic conductivity ($Lp_{r\text{-}h}$) of the wild-type (Col-0) plants (n = 5). (**b**) $Lp_{r\text{-}o}$ of Col-0 roots treated with 1 µM IAA for 18 h and 42 h was determined. Data shown are mean value ± sem with n =14, 14, 15 from 2 independent plant cultures..(**c**) The *arf7* mutant $Lp_{r\text{-}h}$ is strongly affected by a H_2O_2 treatment (5 mM for 20 min) The mean of 2 experiments is shown.(NT, non-treated roots (**d-f**) Water relation parameters were determined in single root cortical cells of non-treated plants (NT) or plants treated with 1 µM IAA for 18 hours (IAA). Cell hydraulic conductivity was calculated from the half-time of water exchange ($T_{1/2}$) (d), the stationary turgor pressure (e) and the volumetric elastic modulus (Epsilon) (f) (n = 22) (**g-h**) Characterization of free sap exudation in roots from wild type (Col-0) and *pip1;2-2* mutant plants complemented (*pip2;1-2* PIP2;1) or not (*pip2;1-2*) with a *PIP2;1* genomic fragment. Sap flow rate (g) and osmolarity (h) was used to deduce the $Lp_{r\text{-}h}$ $Lp_{r\text{-}o}$ values shown in Fig. 2f. Data shown are mean value ± sem from 2 independent plant cultures (n=21, 18, 22). (**i, j**) $Lp_{r\text{-}h}$ (i), data shown are mean value ± sem with n =35, 13, 18 from 2 independent plant cultures and $Lp_{r\text{-}o}$ (j), data shown are mean value ± sem with n =27, 21, 14 from 3 independent plant cultures, of Col-0 and single or double knock-outs for *PIP2;1* (*pip2;1*) and *PIP2;2* (*pip2;2*). Asterisks indicate a significant difference with corresponding control experiment by Student's t-test (*: $p < 0.05$; **: $p < 0.01$; ***: $p < 0.001$).

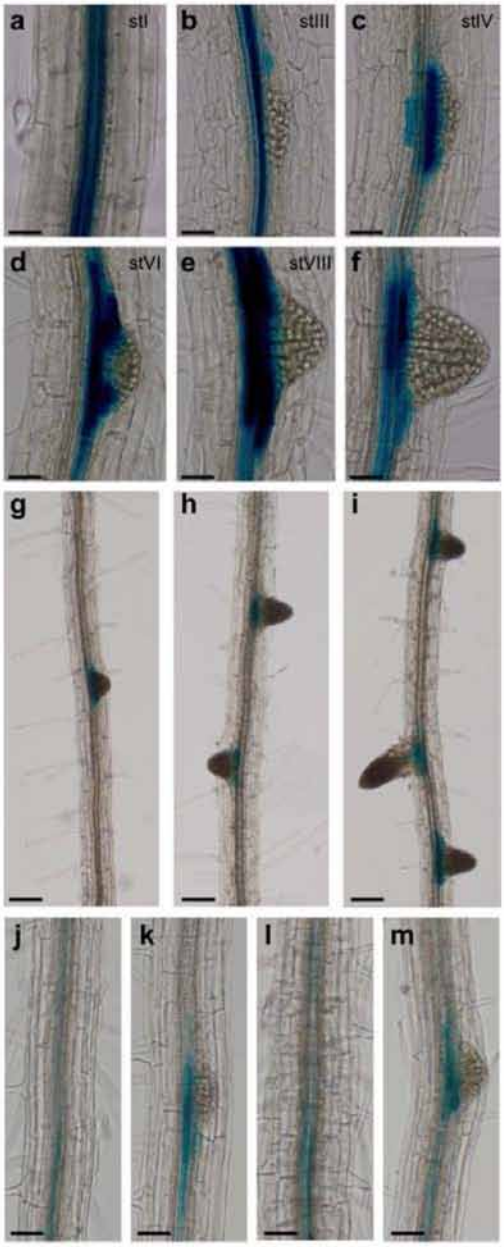

Figure S3 Characterization of the *PIP2;8::GUS* reporter lines. (**a-f**) *PIP2;8* expression determined with a transcriptional *proPIP2;8:GUS* fusion during lateral root development. LR developmental stages are indicated by Roman numbers as described previsouly[20]. Expression pattern was verified with three independent transgenic lines. (**g-m**) Auxin and anti-auxin treatments did not affect *proPIP2;8:GUS* expression pattern. Untreated 7 day-old plants (g, j, k), plants treated with 1 µM IAA for 48 hours (h,i) and plants treated with 10 µM PCIB for 24 hours (l,m). The results were verified using an independent transgenic line. Scale bars represent 50 µm (a-f), 75 µm (j-m) and 100 µm (g-i).

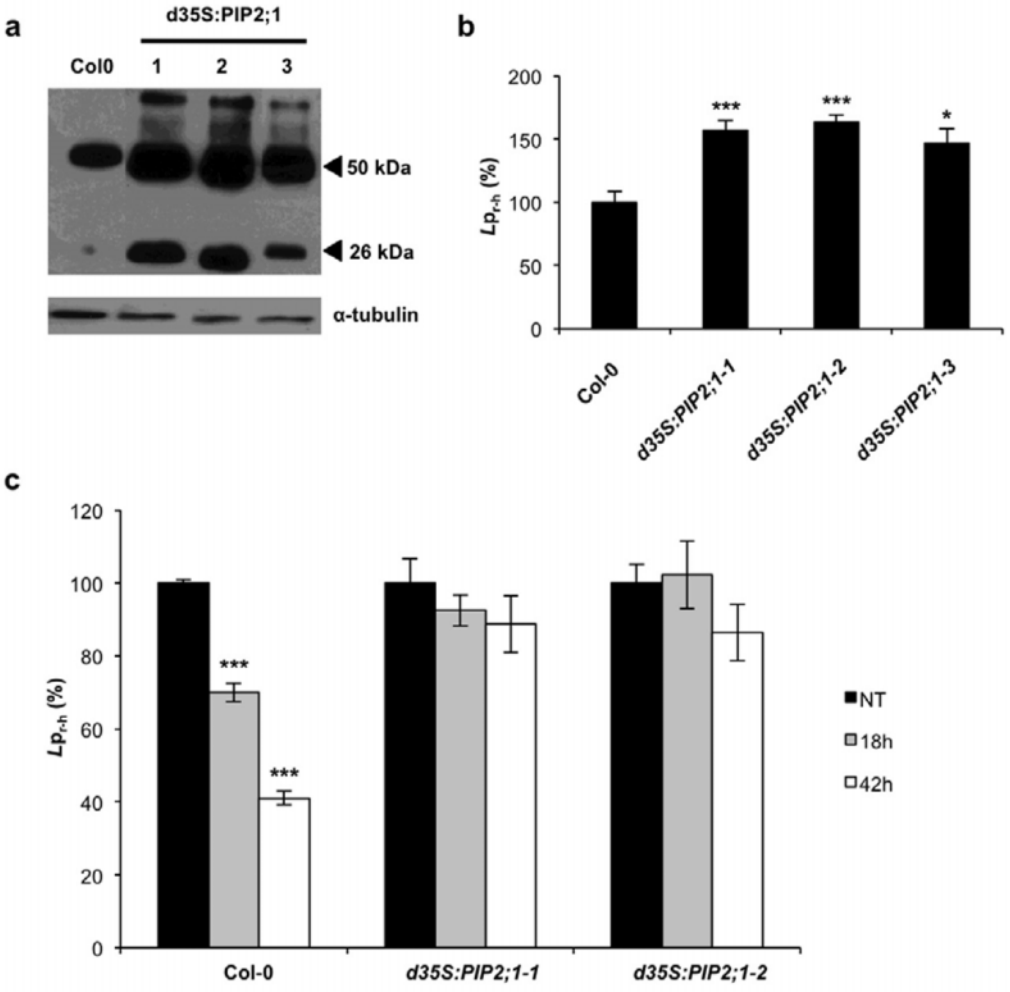

Figure S4 Characterization of the *PIP2;1* over-expression lines. (**a**) Western blot of three independent *d35S:PIP2;1* lines (lanes 1 to 3) showing strong accumulation of the PIP2 proteins compared to wild type (Col-0). The two bands correspond to monomeric and dimeric forms. Representative experiment with 5 µg proteins per lane. ELISA assays on the same samples showed that, with respect to Col-0, proteins immunoreactive to the anti-PIP2 antibody were increased by 2.6-2.9-fold in the *d35S:PIP2;1* lines (**b**) Hydrostatic root hydraulic conductivity (Lp_{r-h}) is increased in three independent *d35S:PIP2;1* lines (1 to 3). Data shown are mean value ± sem with n =21, 20, 17, 16 from 3 independent plant cultures (**c**) The reduction of root hydraulic conductivity by auxin is suppressed in the *PIP2;1* over-expression lines. Lp_{r-h} was determined upon 18 and 42 hours treatments with 1 µM IAA and indicated as a percentage of untreated control. Data shown are mean value ± sem with n =21, 13, 19, 9, 8, 12, 7, 6, 10 from 2 independent plant cultures. Asterisks indicate a significant difference with corresponding control experiment by Student's t-test (*: $p < 0.05$; ***: $p < 0.001$).

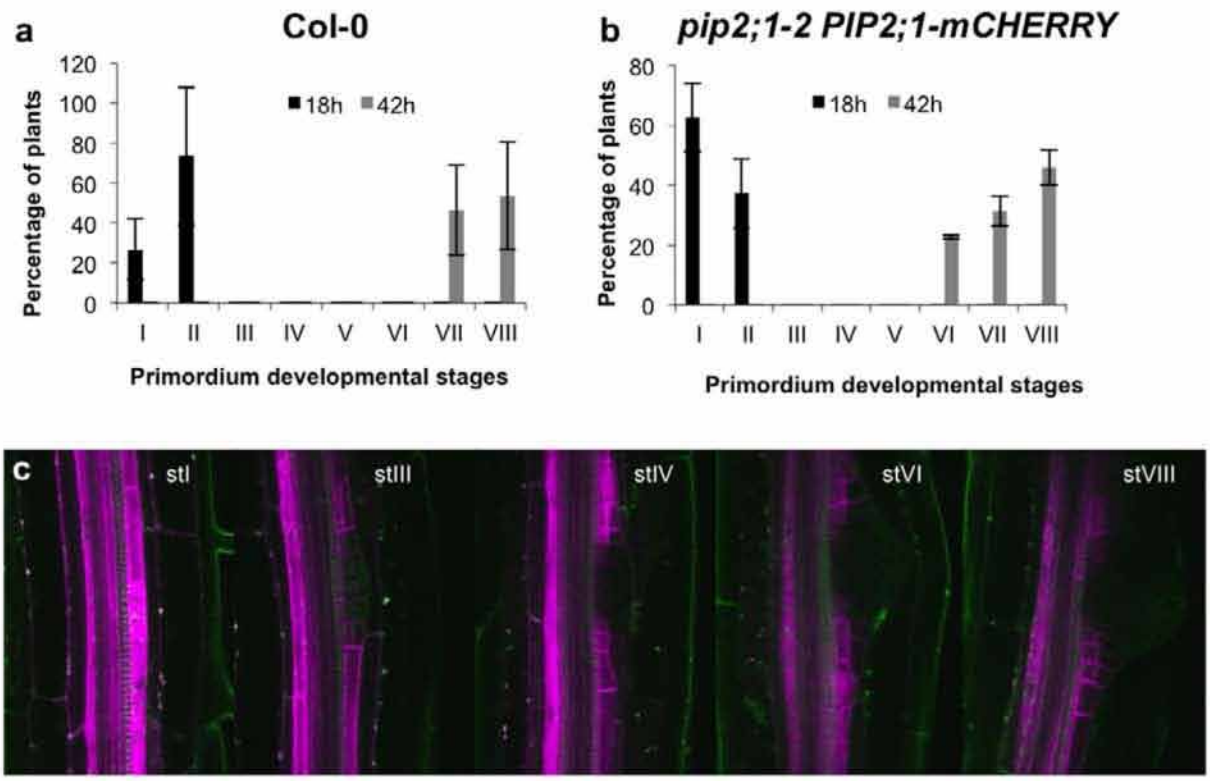

Figure S5 The PIP2;1-mCHERRY fusion rescues the *pip2;1* LR emergence phenotype. (**a-b**) Expressing the *proPIP2;1:PIP2;1-mCHERRY* construct in the *pip2;1-2* mutant background (b) restores kinetics of LR emergence similar to those in wild-type (Col-0, a). (**c**) Expression pattern driven by the *proPIP2;1:PIP2;1-mCHERRY* construct in the *pip2;1-2* background is similar to the expression driven when expressing the same construct in the wild-type (Col-0) background (as shown in Figure 3d).

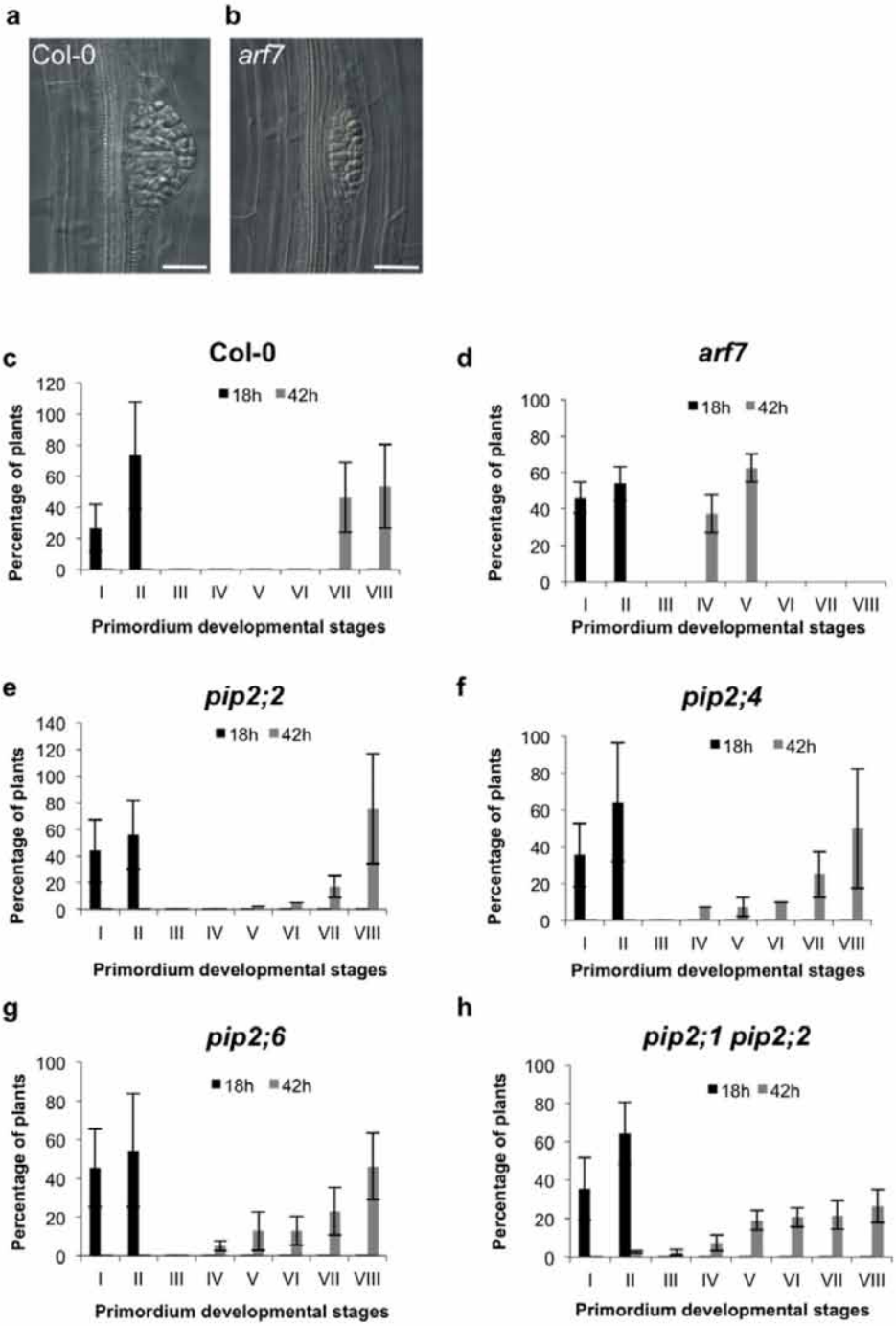

Figure S6 Lateral root emergence is defective in *arf7* mutants and in single or multiple *pip2* mutants. LRE phenotyping was achieved by synchronizing LR formation with a gravistimulus (**a,b**) Differential interference contrast imaging at 42 hours post-induction (hpi) showed abnormal LR primordia of *arf7* mutants (b) compared to dome-shaped wild-type primordium (a). Scale bars represent 25 µm (**c-h**) Primordia were grouped according to developmental stages as previously defined[20] 18 hpi (black bars) and 42 hpi (grey bars). (**c**) Wild-type (Col-0) plants showed accumulation of stage I and II primordium 18 hpi and accumulation of stage VII and VIII 42 hpi. (**d**) *arf7* mutants showed similar stages of LR formation at 18 hpi compared to wild type thereby suggesting that early stages of LR development were not affected. However, most LRP accumulated at stage IV and V 42 hpi indicating a strong emergence defect. (**c-e**) The *pip2;2, pip2;4 and pip2;6* single mutants and the double *pip2;1 pip2;2* mutant showed similar stages of LR formation at 18 hpi compared to wild type thereby suggesting that early stages of LR development were not affected. However, they present an accumulation of stages IV to VI LR primordia at 42 hpi indicating an emergence defect. The double *pip2;1 pip2;2* mutant (h) also showed a reduced amount of LRP reaching stage VIII at 42 hpi Data shown are mean value ± sem and n = 20 (c-h).

AGI	Primer name	Primer sequence
At3g61430	qPIP1;1F	CTGGCCTTGTCCTTAGTTGCTTC
	qPIP1;1R	TCTCCTTTGGAACTTCTTCCTTG
At2g45960	qPIP1;2F	TCCTCTTCTTTGCCTAATGGAGAC
	qPIP1;2R	AGTTGCCTGCTTGAGATAAAC
At1g01620	qPIP1;3F	GCTGTGGATGATCTGGTTTTATCG
	qPIP1;3R	GCCGAAACAATATGGATCTTACTC
At4g00430	qPIP1;4F	CTCTGAAGTCTAAGGTGATTAGTGC
	qPIP1;4R	CAACCCGAGAACTTGATGTTGA
At4g23400	qPIP1;5F	TGTTTCCTATGTCATGTGTGATG
	qPIP1;5R	GTACACAATGTATTCTTCCATTGAC
At3g53420	qPIP2;1F	TGTGTTTTCCACTTGCTCTTTTG
	qPIP2;1R	CACAACGCATAAGAACCTCTTTGA
At2g37170	qPIP2;2F	GGCAACTTTGCTTGTAAAACTATGC
	qPIP2;2R	AGTACACAAACATTGGCATTGG
At2g37180	qPIP2;3F	GAAACATATCCTCTTTTCCACTCG
	qPIP2;3R	CTCAATACACCAAACTTACATACG
At5g60660	qPIP2;4F	CTCCTTTAGGAGCTTTGCTTAAT
	qPIP2;4R	CCACATTTACAATTACACGAATGG
At3g54820	qPIP2;5F	GATATGCTCTTCCCTGAGTACATC
	qPIP2;5R	AATATCTCTCCTCACCAAAGCTAG
At2g39010	qPIP2;6F	TTTCGAACTAGCGAAGAGGTGAAG
	qPIP2;6R	AGACACAGTAAATGTCACTCACC
At4g35100	qPIP2;7F	TGTGTAATGAGAGAGATGGTGGA
	qPIP2;7R	AGAGAAACCAAAGGCAAACGA
At2g16850	qPIP2;8F	CAACCCAACCAATTGATGATTCA
	qPIP2;8R	ACATGAAAGAAAGCAACGGAC
At2g36830	qTIP1;1F	CTCCCAACCACAGACTACTGAA
	qTIP1;1R	GCACGATCATAAACCCCTTG
At3g26520	qTIP1;2F	GCATCGTAATGGGTTTCTGG
	qTIP1;2R	TACAATTGCACAAAAGCCTTCC
At4g17340	qTIP2;2F	AGCTCCCACCACAGAAAGCTA
	qTIP2;2R	TTTGGAAGAAACGAGGACCA
At5g47450	qTIP2;3F	GTGAGATCCGAGTGTAATTGACTG
	qTIP2;3R	TTTTCTTTTCTCTACATACAATCTTGC

Figure S7 List of primers used for quantitative RT-PCR. Primer sequences are given from 5' to 3'.

Supplementary model description for 'Auxin regulates aquaporin function to facilitate lateral root emergence'

1 Model description

In this text, we provide further details of the development and predictions of our tissue-scale mathematical model that seeks to describe key aspects of the biomechanics of lateral root emergence. As detailed in the main text, we have experimental evidence that auxin represses aquaporin expression during lateral root development. However, how this repression affects the water fluxes and turgor pressure and how these combine to influence emergence is not readily accessible to intuition but is well-suited to mechanistic modelling. The model developed here shows how auxin's repression of aquaporins influences the biomechanics of emergence and provides further insight into our experimental results. We also use the model to investigate the observed spatial distribution of the PIP2;1 aquaporin, which we have shown to be highly expressed in lateral root primordia and to contribute significantly to root hydraulic conductivity (see figures 2f and 3a,d,b, main text, and supplementary figure S2g,h). In the wild-type plants, PIP2;1 is present in the stele and primordium prior to emergence; during emergence, PIP2;1 levels are maintained in the stele whilst auxin accumulation causes the PIP2;1 level in the primordium to reduce (see figure 3 in the main text). To assess whether this spatial distribution facilitates emergence, we use the model to simulate the dynamics in the *pip2;1* knockout mutant and the d35S;PIP2;1 over-expression mutant. The model predicts, somewhat counterintuitively, that both mutations result in delayed emergence, thereby providing distinct predictions which we verified experimentally.

The model, which seeks to provide the simplest mathematical representation of the key phenomena, describes the formation of the lateral root from a stage I primordium to emergence occurring at stage VIII (using the lateral root stages defined in Malamy *et al.* (1997)). We consider the cross-section of the root (*i.e.* a slice through the tissue perpendicular to the root axis) and the region encompassing the primordium and overlaying cells, as shown in figure M1. Rather than simulate individual cells, we use a compartmental approach (an approach that is used frequently in root water-uptake modelling, as described by Murphy (2000, 2003) and references therein). Thus, our model considers two tissue regions that we represent as homogeneous fluid-like compartments, namely the growing primordium and the overlaying tissue, see figure

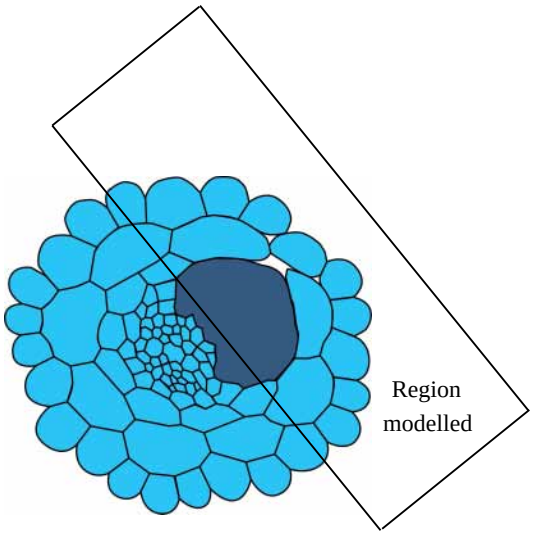

Figure M1: A root cross-section featuring an emerging primordium, drawn from a confocal image. The label shows the region (*i.e.* the primordium and overlaying tissue) that is considered in the model.

M2. We lump the effects of cell-wall extension and cell-to-cell reorganisation into the boundaries surrounding each tissue region, allowing the pressures within each region (averaged over the component cells) to be treated as spatially uniform. We denote the hydrostatic pressure in each region at time t by $P_j(t)$ and the osmotic potential by $\pi_j(t)$, where subscript $j = 1$ refers to the primordium and $j = 2$ to the overlaying cells. Without loss of generality, we take the hydrostatic pressure and osmotic potential to be zero external to the root, so that the pressures within the root are considered relative to those in the external environment. We assume that emergence is driven by changes in osmotic potential: as cells divide within the primordium, the osmotic potential will increase, drawing water into the primordium (Bressan *et al.*, 1982); these water fluxes result in a build-up in hydrostatic pressure which, as we shall show, can be interpreted as leading to lateral root emergence. In the model, we therefore prescribe the primordium's osmotic potential prior to $t = 0$ to be $\pi_1 = \pi_{1\text{init}}$; then, for definiteness, we prescribe π_1 to be linearly increasing at some rate π_{1g}, such that:

$$\pi_1(t) = \pi_{1\text{init}} + \pi_{1g}t. \tag{1.1}$$

We capture effects of cell-wall extension and cell-to-cell reorganisation by modelling each boundary as a sheet of Bingham material, which will lengthen if the tangential stress, due to a hydrostatic pressure difference across the boundary, is greater than some yield stress (*cf.* the Lockhart equation (Lockhart, 1965)). Letting $j = 1, 2$ label the sheets, we denote their viscosities by μ_j, yield stresses by Γ_j and lengths by $l_j(t)$. For simplicity, we assume that the material properties are constant and neglect any weakening of

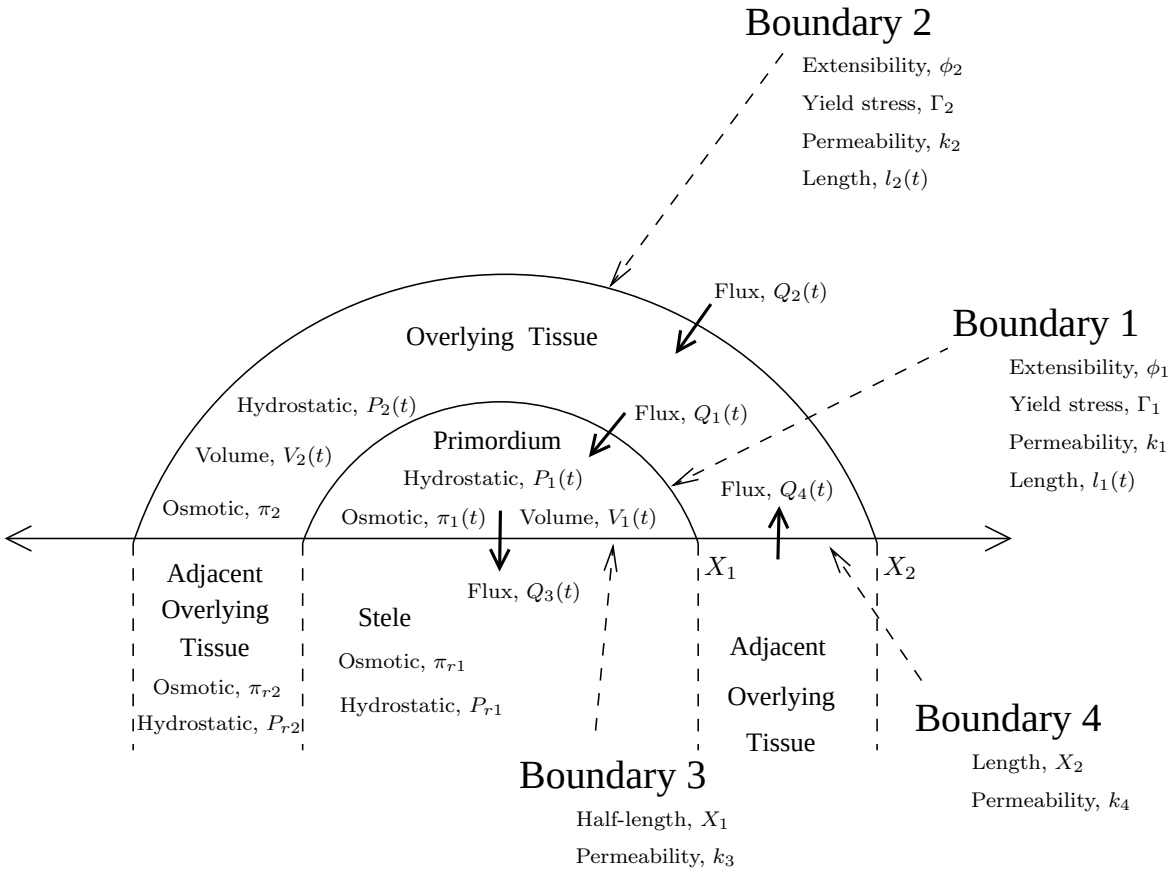

Figure M2: Schematic for the two-dimensional two-compartment model of the cross-section of the root tissue (*i.e.* a slice perpendicular to the axis of the root). The model consists of two regions of tissue, representing the primordium and the overlaying tissue.

the tissue overlaying the primordium[1]. In addition, we follow Dyson & Jensen (2010) in supposing that new material is deposited as the boundaries lengthen so that both have a constant thickness, denoted by h.

Since we ignore variations in the third spatial dimension and any pressure gradients along the sheet, a tangential force balance shows that the tangential stress within the sheet is spatially uniform (*i.e.* does not depend on the distance along the sheet). Thus, labelling the tangential stress within each sheet by σ_j, the boundaries lengthen according to[2] Dyson & Jensen (2010).

$$\sigma_j - \Gamma_j = \frac{4\mu_j h}{l_j}\frac{\mathrm{d}l_j}{\mathrm{d}t} \quad \text{provided} \quad \sigma_j - \Gamma_j > 0. \tag{1.2}$$

The force balance normal to the sheet takes the form of the Young-Laplace law, which implies that the hydrostatic pressure difference across a sheet equals its tangential stress times its curvature. Thus, in keeping with the assumptions that the tangential stress and pressure difference are spatially uniform, the curvature is also spatially uniform *i.e.* the sheets form arcs of cylinders. We adopt a Cartesian co-ordinate system and suppose the sheets to be pinned at $(\pm X_j, 0)$ (see figure M2). The sheet positions can then be defined in terms of their radii of curvature, $R_j(t)$ (see figure M3), such that

$$P_2 = \frac{\sigma_2}{R_2}, \quad P_1 - P_2 = \frac{\sigma_1}{R_1}. \tag{1.3}$$

Eliminating σ_j from (1.2) shows that each boundary lengthens according to

$$\frac{\mathrm{d}l_1}{\mathrm{d}t} = \phi_1 l_1 H_1\big(R_1(P_1 - P_2) - \Gamma_1\big), \quad \frac{\mathrm{d}l_2}{\mathrm{d}t} = \phi_2 l_2 H_2\big(R_2 P_2 - \Gamma_2\big), \tag{1.4}$$

where $\phi_j = 1/(4\mu_j h)$ (for $j = 1, 2$) denote the effective extensibilities of the two sheets, and the H_j denote parameters such that

$$H_1 = \begin{cases} 1 & \text{if} \quad R_1(P_1 - P_2) > \Gamma_1, \\ 0 & \text{otherwise,} \end{cases} \qquad H_2 = \begin{cases} 1 & \text{if} \quad R_2 P_2 > \Gamma_2, \\ 0 & \text{otherwise.} \end{cases} \tag{1.5}$$

Expansion of each region requires water fluxes, which are driven by the differences in hydrostatic pressure and osmotic potential (Kramer & Boyer, 1995; Boyer & Silk, 2004; Dumais & Forterre, 2012). Denoting the permeabilities of the four boundaries bounding the two tissue compartments by k_i (for $i = 1, 2, 3, 4$), as shown in figure M2, the volumes (per unit length) of the two regions satisfy

$$\frac{\mathrm{d}V_1}{\mathrm{d}t} = l_1 Q_1 - 2X_1 Q_3, \tag{1.6a}$$

$$\frac{\mathrm{d}V_2}{\mathrm{d}t} = l_2 Q_2 - l_1 Q_1 + 2(X_2 - X_1) Q_4, \tag{1.6b}$$

[1] Although the presence of auxin may cause gradual weakening (Swarup *et al.*, 2008), we focus here on constructing a minimal model that describes how emergence is affected by changes in aquaporin activity.

[2] Note that the factor of 4 arises in (1.2) from the standard Trouton viscosity model, see for example Van der Fliert *et al.* (1995).

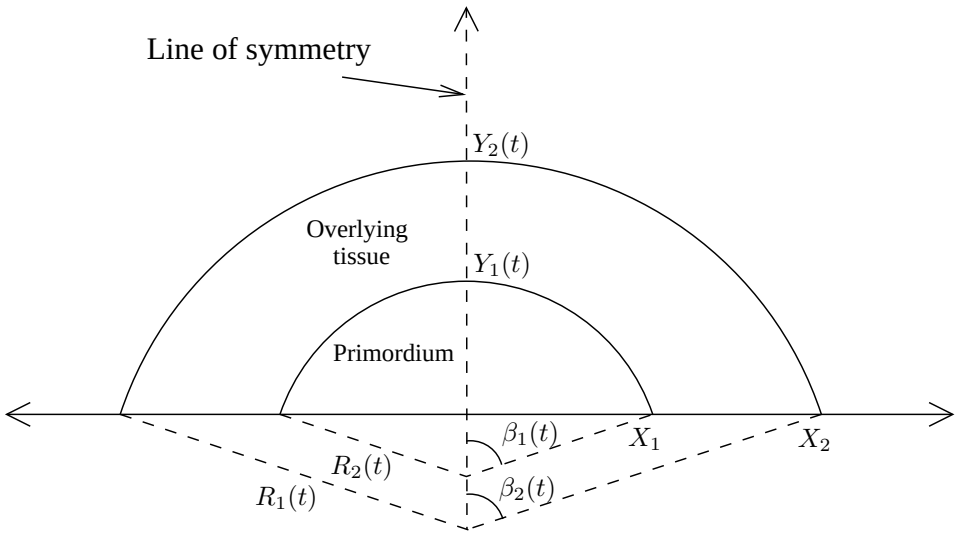

Figure M3: The sheets each form an arc of a cylinder which has radius $R_j(t)$ and which meets the x-axis at $(\pm X_j, 0)$.

where the fluxes per unit length are given by

$$Q_1 = k_1(P_2 - P_1 - \pi_2 + \pi_1), \qquad Q_2 = k_2(-P_2 + \pi_2), \tag{1.7a}$$

$$Q_3 = k_3(P_1 - P_{r1} - \pi_1 + \pi_{r1}), \qquad Q_4 = k_4(P_{r2} - P_2 - \pi_{r2} + \pi_2). \tag{1.7b}$$

Here, P_{r1} and π_{r1} respectively denote the hydrostatic pressure and osmotic potential of the vasculature tissue which lies adjacent to the primordium, and P_{r2} and π_{r2} are the hydrostatic pressure and osmotic potential of the outer layers of the root that lie adjacent to the overlaying tissue. The values of the permeabilities, and hence the magnitude of the fluxes, depend on whether aquaporins are functional (Javot & Maurel, 2002). As described in the main text, auxin accumulation causes a reduction in aquaporin expression (figures 1e, 2a,b) and activity (figures 2c,d). Therefore, we capture the effects of auxin accumulation in the primordium and overlaying tissue by prescribing a gradual reduction in the permeabilities of boundaries 1 and 2; as illustrated in figure M4, we let

$$k_j = \max\big(k_{j\text{init}}(1 - k_{jg}t), k_{j\text{min}}\big) \quad \text{for} \quad j = 1, 2, \tag{1.8}$$

where $k_{j\text{init}}$ denote the permeabilities at $y = 0$, k_{jg} represent the rates at which the permeabilities reduce and $k_{j\text{min}}$ are the permeabilities of the boundaries when all aquaporins are repressed (*i.e.* the minimum permeability).

Since the viscous sheets form arcs of cylinders, the position of each wall can be specified in terms of the angles $\beta_j(t)$, shown in figure M3, and we find these convenient variables to use for the model simulations.

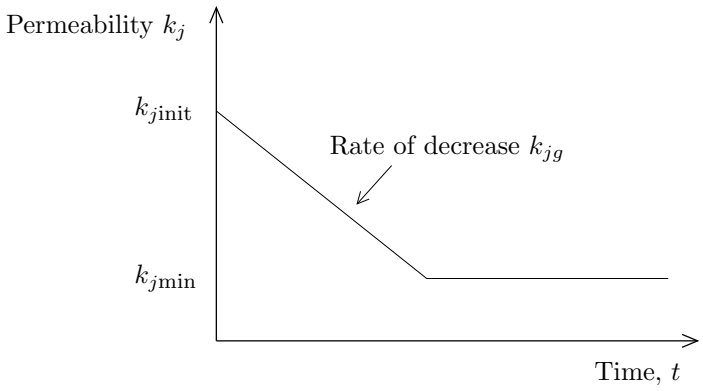

Figure M4: Sketch of the dynamics of k_j for $j = 1, 2$. Auxin accumulation causes the permeabilities of boundaries 1 and 2 to reduce; for each boundary, we prescribe the reduction using three parameters, $k_{j\text{init}}$, k_{jg} and $k_{j\text{min}}$, as illustrated here.

Simple geometric rules enable us to write down the compartment volumes, V_j, and the lengths, l_j, radii of curvature, R_j, and maximum heights, Y_j, of the two boundaries, in terms of the two variables $\beta_j(t)$ and two constants X_j:

$$V_1 = X_1^2\left(\frac{\beta_1}{\sin^2\beta_1} - \frac{\cos\beta_1}{\sin\beta_1}\right), \quad V_2 = X_2^2\left(\frac{\beta_2}{\sin^2\beta_2} - \frac{\cos\beta_2}{\sin\beta_2}\right) - X_1^2\left(\frac{\beta_1}{\sin^2\beta_1} - \frac{\cos\beta_1}{\sin\beta_1}\right), \tag{1.9a}$$

$$l_j = \frac{2X_j\beta_j}{\sin\beta_j}, \quad R_j = \frac{X_j}{\sin\beta_j}, \quad Y_j = \frac{X_j}{\sin\beta_j}(1-\cos\beta_j) \quad \text{for} \quad j = 1, 2. \tag{1.9b}$$

Equations (1.4, 1.6) can then be manipulated to form a system of four equations that govern the remaining four variables, namely the boundary positions, $\beta_j(t)$, and the pressures, $P_j(t)$. Substituting (1.9) into the governing equations, (1.4), we obtain two ordinary differential equations (ODEs) for $\beta_j(t)$:

$$\frac{\mathrm{d}\beta_1}{\mathrm{d}t} = \frac{\phi_1 H_1\beta_1\sin\beta_1}{(\sin\beta_1 - \beta_1\cos\beta_1)}\left(\frac{X_1(P_1-P_2)}{\sin\beta_1} - \Gamma_1\right), \tag{1.10a}$$

$$\frac{\mathrm{d}\beta_2}{\mathrm{d}t} = \frac{\phi_2 H_2\beta_2\sin\beta_2}{(\sin\beta_2 - \beta_2\cos\beta_2)}\left(\frac{X_2P_2}{\sin\beta_2} - \Gamma_2\right). \tag{1.10b}$$

Substituting (1.9) into the governing equations (1.6) also gives two ODEs for $\beta_j(t)$; however, these can be simplified using (1.10) to form two transcendental equations:

$$\frac{\phi_1 H_1 X_1^2\beta_1}{\sin^2\beta_1}\left(\frac{X_1(P_1-P_2)}{\sin\beta_1} - \Gamma_1\right) = \frac{X_1\beta_1}{\sin\beta_1}Q_1 - X_1Q_3, \tag{1.11a}$$

$$\frac{\phi_2 H_2 X_2^2\beta_2}{\sin^2\beta_2}\left(\frac{X_2P_2}{\sin(\beta_2)} - \Gamma_2\right) - \frac{\phi_1 H_1 X_1^2\beta_1}{\sin^2\beta_1}\left(\frac{X_1(P_1-P_2)}{\sin\beta_1} - \Gamma_1\right) = \frac{X_2\beta_2}{\sin\beta_2}Q_2 - \frac{X_1\beta_1}{\sin\beta_1}Q_1 + (X_2 - X_1)Q_4. \tag{1.11b}$$

Thus, the emergence dynamics can be described by the system (1.10, 1.11).
We suppose that the model is initially at a steady state (with neither boundary yielding) and then evolves as the osmotic potential of the primordium increases, (1.1). Steady solutions have $H_j = 0$ and pressures, P_j, which can be calculated via expressions (1.7) and

$$\frac{\beta_1}{\sin\beta_1}Q_1 - Q_3 = 0, \quad \frac{X_2\beta_2}{\sin\beta_2}Q_2 - \frac{X_1\beta_1}{\sin\beta_1}Q_1 + (X_2 - X_1)Q_4 = 0. \tag{1.12}$$

In steady state, the volumes of the tissue compartments are fixed but there may be steady fluxes of water between them. Thus, we must ensure that the chosen parameters satisfy

$$\frac{X_1(P_1(0) - P_2(0))}{\sin(\beta_1(0))} - \Gamma_1 < 0, \quad \frac{X_2P_2(0)}{\sin(\beta_2(0))} - \Gamma_2 < 0, \tag{1.13}$$

where $P_j(0)$ are solutions of equations (1.7, 1.12) with $\beta_1 = \beta_1(0)$ and $\beta_2 = \beta_2(0)$.
As summarised in Table 1, the model depends on the parameters X_j, P_{rj}, π_j, π_{rj}, ϕ_j, $k_{j\text{init}}$, k_{jg}, $k_{j\text{min}}$, k_3, k_4 and Γ_j, together with the initial positions of the boundaries, $\beta_j(0)$ (where $j = 1, 2$). Biological motivation for the parameter values will be discussed in detail in §3. Having specified the parameters, simulations of the model predict how the pressures and boundary positions evolve, and can be used to show how the emergence dynamics are affected by the parameter choices (§4). In particular, we will focus on how auxin influences emergence by reducing the permeabilities of boundaries 1 and 2 (via k_{1g} and k_{2g} respectively). We will also use the model to investigate the importance of the PIP2;1 distribution (shown in figure 3, main text). We will consider i) an ectopic PIP2;1 distribution (*i.e.* the d35S;PIP2;1 over-expression mutant), by removing auxin's influence ($k_{jg} = 0$) and increasing the permeabilities of boundaries 2 and 4 ($k_{2\text{init}}$ and k_4), and ii) the *pip2;1* knockout mutant, by removing auxin's influence on boundary 1 ($k_{1g} = 0$) and reducing the permeabilities of boundaries 1 and 3 ($k_{1\text{init}}$ and k_3).

2 Nondimensionalisation

To gain understanding of the dynamics, we nondimensionalise the model – this being a standard mathematical technique which enables the model to be expressed in terms of a reduced number of (dimensionless) parameter groupings that characterise the behaviour. Since a number of the model parameter values have not been accurately measured, nondimensionalising is beneficial in reducing the parameter space of the model. We nondimensionalise the variables in the system according to

$$(P_j, \pi_1) = \pi_{1\text{init}}(P_j^*, \pi_1^*), \quad (l_j, Y_j) = X_1(l_j^*, Y_j^*), \quad Q_i = k_{\text{typ}}\pi_{1\text{init}}Q_i^*, \quad t = \frac{X_1 t^*}{\pi_{1\text{init}}k_{\text{typ}}}, \tag{2.1}$$

for $i = 1, 2, 3, 4$, $j = 1, 2$, where asterisks are used to denote the dimensionless variables. For convenience, we have introduced a typical boundary permeability, k_{typ}: we take this parameter equal to the wild-type value $k_{2\text{init}}$, enabling us to vary each permeability independently when considering the behaviour of the mutants. We express hydrostatic pressures and osmotic potentials in terms of the initial osmotic potential

of the primordium, $\pi_{1\text{init}}$, lengths in terms of the half length of the base of the primordium, X_1, fluxes in terms of a typical flux, $\pi_{1\text{init}}k_{\text{typ}}$, and time relative to the typical time scale of water fluxes, $X_1/(\pi_{1\text{init}}k_{\text{typ}})$. With this nondimensionalisation, the model depends on 19 dimensionless parameter groupings (which we again denote with asterisks),

$$X_2^* = \frac{X_2}{X_1}, \quad \phi_2^* = \frac{\phi_2}{\phi_1}, \quad (k_i^*, k_{j\text{init}}^*, k_{j\text{min}}^*) = \frac{1}{k_{\text{typ}}}(k_i, k_{j\text{init}}, k_{j\text{min}}), \quad k_{jg}^* = \frac{X_1 k_{jg}}{\pi_{1\text{init}}k_{\text{typ}}},$$
$$\Gamma_j^* = \frac{\Gamma_j}{X_1\pi_{1\text{init}}}, \quad T^* = \frac{\phi_1 X_1^2}{k_{\text{typ}}}, \quad \pi_{1g}^* = \frac{X_1\pi_{1g}}{\pi_{1\text{init}}^2 k_{\text{typ}}}, \quad (P_{rj}^*, \pi_{rj}^*, \pi_2^*) = \frac{1}{\pi_{1\text{init}}}(P_{rj}, \pi_{rj}, \pi_2), \tag{2.2}$$

for $i = 3, 4$ and $j = 1, 2$. The parameter T^* gives the ratio between the typical time scales for water fluxes and expansion. In addition, we let

$$\pi_1^* = \frac{\pi_1}{\pi_{1\text{init}}}, \quad k_j^* = \frac{k_j}{k_{\text{typ}}}, \tag{2.3}$$

for $j = 1, 2$, so that from (1.1) and (1.8)

$$\pi_1^*(t^*) = 1 + \pi_{1g}^* t^*, \quad k_j^*(t^*) = \max\bigl(k_{j\text{init}}^*(1 - k_{jg}^* t^*), k_{j\text{min}}^*\bigr). \tag{2.4}$$

With (2.1) and (2.2), the governing equations, (1.10, 1.11), become

$$\frac{\mathrm{d}\beta_1}{\mathrm{d}t^*} = \frac{T^* H_1 \beta_1 \sin\beta_1}{(\sin\beta_1 - \beta_1\cos\beta_1)}\left(\frac{(P_1^* - P_2^*)}{\sin\beta_1} - \Gamma_1^*\right), \tag{2.5a}$$
$$\frac{\mathrm{d}\beta_2}{\mathrm{d}t^*} = \frac{T^* H_2 \phi_2^* \beta_2 \sin\beta_2}{(\sin\beta_2 - \beta_2\cos\beta_2)}\left(\frac{X_2^* P_2^*}{\sin\beta_2} - \Gamma_2^*\right), \tag{2.5b}$$
$$\frac{T^* H_1 \beta_1}{\sin^2\beta_1}\left(\frac{(P_1^* - P_2^*)}{\sin\beta_1} - \Gamma_1^*\right) = \frac{\beta_1}{\sin\beta_1}Q_1^* - Q_3^*, \tag{2.5c}$$
$$\frac{\phi_2^* T^* H_2 \beta_2 X_2^{*2}}{\sin^2\beta_2}\left(\frac{X_2^* P_2^*}{\sin\beta_2} - \Gamma_2^*\right) - \frac{T^* H_1 \beta_1}{\sin^2\beta_1}\left(\frac{(P_1^* - P_2^*)}{\sin\beta_1} - \Gamma_1^*\right)$$
$$= \frac{X_2^*\beta_2}{\sin\beta_2}Q_2^* - \frac{\beta_1}{\sin\beta_1}Q_1^* + (X_2^* - 1)Q_4^*, \tag{2.5d}$$

with

$$Q_1^* = k_1^*(P_2^* - P_1^* - \pi_2^* + \pi_1^*), \quad Q_2^* = k_2^*(-P_2^* + \pi_2^*), \tag{2.6a}$$
$$Q_3^* = k_3^*(P_1^* - P_{r1}^* - \pi_1^* + \pi_{r1}^*), \quad Q_4^* = k_4^*(P_{r2}^* - P_2^* - \pi_{r2}^* + \pi_2^*). \tag{2.6b}$$

and

$$H_1 = \begin{cases} 1 & \text{if} \quad (P_1^* - P_2^*)/\sin\beta_1 > \Gamma_1^*, \\ 0 & \text{otherwise,} \end{cases} \qquad H_2 = \begin{cases} 1 & \text{if} \quad X_2^* P_2^*/\sin\beta_2 > \Gamma_2^*, \\ 0 & \text{otherwise.} \end{cases} \tag{2.7}$$

Prior to yielding, the boundaries are stationary ($\beta_1 = \beta_1(0)$, $\beta_2 = \beta_2(0)$) and the pressures are solutions of a simpler set of linear equations:

$$\frac{\beta_1(0)}{\sin\beta_1(0)}Q_1^* - Q_3^* = 0, \qquad \frac{X_2^*\beta_2(0)}{\sin\beta_2(0)}Q_2^* - \frac{\beta_1(0)}{\sin\beta_1(0)}Q_1^* + (X_2^* - 1)Q_4^* = 0, \tag{2.8}$$

where the fluxes, Q_i^*, are given by (2.6). Further manipulations are possible: supposing, for example, that boundary 1 yields earlier than boundary 2, one could determine yielding time by solving equations (2.8) together with the condition $(P_1^* - P_2^*) = \sin(\beta_1(0))\Gamma_1^*$. Finally, to ensure the model has a legitimate initial steady state, we require

$$\frac{(P_1^*(0) - P_2^*(0))}{\sin(\beta_1(0))} - \Gamma_1^* < 0, \quad \frac{X_2^* P_2^*(0)}{\sin(\beta_2(0))} - \Gamma_2^* < 0, \tag{2.9}$$

where the pressures $P_i^*(0)$ are solutions of (2.8).

3 Parameter estimates

We now discuss the parameter values in the model which are available from the biological literature. Parameter X_1 represents the half length of the base of the emerging primordium, and we take this to be $X_1 = 50\,\mu$m. The difference $X_2 - X_1$ is then the thickness of the overlaying tissue at the edge of the primordium, and we take this to be $X_2 - X_1 = 25\,\mu$m.

Typical pressures within root tissue are 0.4 MPa, whereas the sap (in the vasculature) is maintained at an osmolarity of 0.15 MPa, enabling it to draw in water to be supplied throughout the plant (Javot *et al.*, 2003; Postaire *et al.*, 2010). Since the model lumps together the sap in with the vasculature, we take the osmotic potential of the latter to be 0.55 MPa. In addition, we assume that prior to emergence there is no driving pressure gradient between the primordium, overlaying tissue or adjacent outer root layers, and set $\pi_{1\text{init}} = \pi_2 = \pi_{r2} = P_{r1} = P_{r2} = 0.4\,\text{MPa}$. Since we assume that the model is initially in steady state (with the boundaries stationary), the initial pressures in the primordium and overlaying tissue regions, $P_j(0)$, are solutions of (2.8).

The magnitude of the water fluxes depends on the permeabilities of the boundaries. In *Arabidopsis thaliana* plant roots, the conductivity of a single cortical cell has been measured to be around $2.4\times10^{-6}\,\text{m}\,\text{s}^{-1}\,\text{MPa}^{-1}$ (Javot *et al.* (2003) and figure 2d main text). Unfortunately, it is not currently possible to measure the permeabilities of cells that are deeper in the root tissue, and these may be different to that of the cortical cells, since the individual cell permeabilities depend on the distribution and activity of all members of the aquaporin family, which are currently unknown. The effective permeabilities of the boundaries are likely to be smaller than that measured for a single cortical cell, as the model represents the water flows through collections of cells as fluxes between different regions of the tissue. Because boundaries 2 and 4 each comprise about three individual cell boundaries (including those of the cortical cells), we take their permeabilities, $k_{2\text{init}}$ and k_4, and the typical permeability, k_{typ}, to be a third of the single-cortical-cell values. Appropriate values for permeabilities $k_{1\text{init}}$ and k_3 are less clear (as the corresponding boundaries represent many cells located deep within the root tissue). As we shall see, the emergence dynamics depend on the relative sizes of the boundaries' permeabilities, and we find good agreement with experimental measurements if the permeabilities of boundaries 1 and 3 are greater than those of boundaries 2 and 4, suggesting that the level of functional aquaporin may be higher on boundaries 1 and 3 than on boundaries

2 and 4; we set $k_{1\text{init}} = k_3 = 3k_{2\text{init}}$ (see section 4.3 for further details). For boundaries 1 and 2, we assume that the minimum permeabilities (corresponding to repressed aquaporins) are ten times lower, with $k_{j\text{min}} = 0.1k_{j\text{init}}$.

As discussed above, a build-up of auxin causes a reduction in the permeabilities of boundaries 1 and 2 during emergence, characterised by the parameters k_{1g} and k_{2g}; we take k_{1g} to reflect the rate of decrease of PIP2;1 concentration and, using the data from the antibody assay (figure 2b, main text), we estimate $k_{1g} = 3.6 \times 10^{-6}\,\text{s}^{-1}$. In contrast, k_{2g} represents the inhibition of the other members of the aquaporin family that are potentially present in the overlaying tissue. The RT-PCR data (figures 1c,e in the main text) reveals that the expression of many aquaporin genes reduces faster than that of *PIP2;1* both in response to an auxin dose and during lateral root emergence; we therefore assume that the permeability of boundary 2 reduces at five times the rate of that of boundary 1, setting $k_{2g} = 1.8 \times 10^{-5}\,\text{s}^{-1}$.

The model results also depend on the mechanical properties of the sheets that bound the primordium and overlaying tissue, each being characterised by an extensibility, ϕ_j, and a yield, Γ_j. Unfortunately appropriate estimates of these parameters are not available; we demonstrate how these parameters affect the model solutions in section 4.1. The extensibility of boundary 1 determines the relative time scale of the primordium expansion to that of the water fluxes. Although growth is generally assumed to occur slower than water fluxes for single cells (Cosgrove, 1993), we are considering here growth of collections of cells and suppose that the time scales of growth and water fluxes are similar, setting the ratio $T^* = 1$. We confirm that our model results are not affected by this assumption by considering the alternative case of small T^* in section 4.4. For completeness, we take the extensility of boundary 2 to be equal to that of boundary 1, although we show that this parameter does not affect the predicted dynamics (see section 4.1). We find that the yield stress of boundary 1 determines how much the permeabilities affect the emergence time; when small, boundary 1 can extend more easily and perturbing the water fluxes has a more dramatic effect. Setting the yield stress of boundary 1 to be small seems to be appropriate, since the overlaying tissue is thought to be weakened due to the presence of cell-wall remodelling enzymes (Swarup *et al.*, 2008). A reasonably large yield stress for boundary 2 is required, however, to ensure that condition (2.9) is satisfied.

The biological estimates of the dimensional parameter values are summarised in Table 1. Given these estimates, time is nondimensionalised using a scale of 0.043 hours. The resulting dimensionless parameter groupings are summarised in Table 2. As implied above, estimates for a number of these cannot be obtained from the current literature. Extensive investigations of the model results throughout parameter space revealed that, although these estimates affect the predicted emergence time, their values do not significantly affect our key conclusions. In Table 2, we state the values used to produce the model results (*i.e.* figure 4 in the main text). Our experimental measurements suggest that lateral root emergence occurs over 28 hours, since lateral root primordia were at an average stage of 1.6 after 18 hours post gravitropic induction and progressed to an average stage of 7.6 after 42 hours post gravitropic induction (see data in figure 5a in the main text). Therefore, having chosen the other parameters, the rate of increase of osmotic potential in the primordium was adjusted so that emergence occurred in 28 hours.

As discussed above, we use the model to investigate the role of auxin reducing the permeabilities of

Parameter	Description	Value
π_{r1}	Osmotic potential of vasculature	$0.55\,\mathrm{MPa}$
P_{r1}	Turgor pressure of vasculature	$0.4\,\mathrm{MPa}$
π_{r2}	Osmotic potential of adjacent overlaying cells	$0.4\,\mathrm{MPa}$
P_{r2}	Turgor pressure of adjacent overlaying cells	$0.4\,\mathrm{MPa}$
π_2	Osmotic potential of overlaying cells	$0.4\,\mathrm{MPa}$
$\pi_{1\mathrm{init}}$	Initial osmotic potential of primordium	$0.4\,\mathrm{MPa}$
π_{1g}	Rate of increase of osmotic potential of primordium	Unknown
X_1	Half length of primordium base	$50\,\mu\mathrm{m}$
X_2	Half width of tissue	$75\,\mu\mathrm{m}$
ϕ_1	Effective extensibility of boundary 1	Unknown
ϕ_2	Effective extensibility of boundary 2	Unknown
Γ_1	Yield stress of boundary 1	Unknown
Γ_2	Yield stress of boundary 2	Unknown
k_{typ}	Typical boundary permeability	$0.8\times10^{-6}\,\mathrm{m\,s^{-1}\,MPa^{-1}}$
$k_{1\mathrm{init}}$	Initial permeability of boundary 1	$2.4\times10^{-6}\,\mathrm{m\,s^{-1}\,MPa^{-1}}$
$k_{1\mathrm{min}}$	Minimum Permeability of boundary 1	$2.4\times10^{-7}\,\mathrm{m\,s^{-1}\,MPa^{-1}}$
$k_{2\mathrm{init}}$	Initial permeability of boundary 2	$0.8\times10^{-6}\,\mathrm{m\,s^{-1}\,MPa^{-1}}$
$k_{2\mathrm{min}}$	Minimum permeability of boundary 2	$0.8\times10^{-7}\,\mathrm{m\,s^{-1}\,MPa^{-1}}$
k_3	Permeability of boundary 3	$2.4\times10^{-6}\,\mathrm{m\,s^{-1}\,MPa^{-1}}$
k_4	Permeability of boundary 4	$0.8\times10^{-6}\,\mathrm{s^{-1}\,MPa^{-1}}$
k_{1g}	Rate of decrease of boundary 1 permeability due to auxin	$3.6\times10^{-6}\,\mathrm{s^{-1}}$
k_{2g}	Rate of decrease of boundary 2 permeability due to auxin	$1.8\times10^{-5}\,\mathrm{s^{-1}}$

Table 1: Summary of the estimates of the dimensional parameters in the model. As described in §3, plausible estimates are available for all parameters other than π_{1g}, ϕ_1, ϕ_2, Γ_1 and Γ_2.

boundaries 1 and 2 (*i.e.* considering the influence of parameters k^*_{1g} and k^*_{2g}). We also consider the importance of the PIP2;1 distribution by simulating the emergence dynamics in i) the d35S;PIP2;1 over-expression mutant (*i.e.* with ectopic PIP2;1 expression), by letting $k^*_{1g} = k^*_{2g} = 0$ and increasing $k^*_{2\mathrm{init}}$ and k^*_4, and ii) the *pip2;1* knockout mutant, by letting $k^*_{1g} = 0$ and reducing $k^*_{1\mathrm{init}}$ and k^*_3. The magnitudes of the permeability changes in these mutants are unknown, although we find that the specific choices do not affect our key conclusions. For these mutants, our predictions were confirmed experimentally (as described in the main text), providing accurate measurements of the emergence time in each case; we find that the model can mimic the observed emergence times if we use the parameter values stated in Table 3.

Parameter	Description	Value
π^*_{r1}	Relative osmotic potential of vasculature	1.375
P^*_{r1}	Relative turgor pressure of vasculature	1
π^*_{r2}	Relative osmotic potential of adjacent overlaying cells	1
P^*_{r2}	Turgor pressure of adjacent overlaying cells	1
π^*_2	Relative osmotic potential of overlaying cells	1
π^*_{1g}	Rate of increase of osmotic potential of primordium	$0.0001332^\dagger$
X^*_2	Ratio between length scales	1.5
ϕ^*_2	Ratio between boundaries' effective extensibilities	$1^\dagger$
Γ^*_1	Relative yield stress of boundary 1	$0.01^\dagger$
Γ^*_2	Relative yield stress of boundary 2	$3^\dagger$
$k^*_{1\text{init}}$	Initial permeability of boundary 1	3
$k^*_{1\text{min}}$	Minimum permeability of boundary 1	0.3
$k^*_{2\text{init}}$	Initial permeability of boundary 2	1
$k^*_{2\text{min}}$	Minimum permeability of boundary 2	0.1
k^*_3	Permeability of boundary 3	3
k^*_4	Permeability of boundary 4	1
k^*_{1g}	Rate of decrease of boundary 1 permeability due to auxin	5.6×10^{-4}
k^*_{2g}	Rate of decrease of boundary 2 permeability due to auxin	0.0028
T^*	Ratio between key time scales	$1^\dagger$

Table 2: Summary of the parameter groupings in the nondimensionalised model. Where available, estimates of these parameter groupings are obtained using the dimensional parameter values given in Table 1. The parameter groupings for which such estimates are not available are marked with daggers; we note that π^*_{1g} is chosen to ensure emergence occurs over 28 hours. In §4, we discuss how varying the value of each parameter grouping affects the emergence time (see figure M8).

4 Model results

The governing equations, (2.5), are simulated numerically using Matlab, and we provide the numerical code both as a supplementary file and at *www.cpib.ac.uk/tools-resources/models*. We solve equations (2.5a,b) using the in-built ODE solver *ode15s*, with (2.5c,d) solved at each time step using the *fsolve* function. We view the primordium as having emerged when the distance between the two boundaries is less than a prescribed constant, Y_m^* *i.e.* when $Y_2^*(t) - Y_1^*(t) < Y_m^*$ (which we determine numerically using the *Events* option in the ODE solver). In the simulations presented, we use $Y_m^* = 0.08$, unless otherwise stated.

4.1 The emergence dynamics in wild-type plants

In figure M5, we show a typical simulation, using the parameter values stated in Table 2. The model predicts that throughout emergence the prescribed increasing osmotic potential within the primordium (figure M5a) draws in water from the overlaying tissue, $Q_1^* > 0$, (figure M5b). In contrast, the relatively high osmotic potential of the vasculature (together with the evolving hydrostatic pressure in the primordium) cause the flux between the primordium and vasculature to be toward the vasculature, $Q_3^* > 0$ (figure M5c). Meanwhile, water is supplied to the overlaying tissue from both the adjacent tissue and the external environment, $Q_2^* > 0$ and $Q_4^* > 0$ (figure M5b,c).

The model also predicts the evolution of the pressures within the primordium and overlaying tissue. Prior to yielding, the pressures evolve according to (2.8) due to the prescribed time dependence of π_1, k_1 and k_2. We note that the pressures vary nonlinearly with time and that the sudden change in the pressure gradient (at 13.7 hours) occurs when the prescribed decrease of k_2 ceases and k_2 reaches its minimal plateau value. At the beginning of the simulation, the hydrostatic pressure in the overlaying tissue is larger than that in the primordium, due to the flow of water towards the vasculature (driven by its high osmotic potential); however, as the osmotic potential of the primordium increases, the hydrostatic pressure there becomes greater than that in the overlaying tissue (figure M5d), creating tension within boundary 1. Once this becomes larger than the yield stress, boundary 1 begins to lengthen and the volume of the primordium increases. Since we choose the yield stress of boundary 2, Γ_2^*, to be sufficiently large that the initial state is steady, we find that boundary 2 never yields, remaining stationary (figure M5e,f). We note that should we have assumed boundary 2 to be stationary from the outset, our model would be governed by a simpler system of equations: a single ODE (2.5a) and two algebraic expressions (2.5c,d), with H_2=0 and β_2 being a prescribed constant. Eventually (at $t = 28.0$ hours) boundary 1 becomes sufficiently close to boundary 2 that emergence can be taken to have occurred (figure M5e,f).

The magnitude of each water flux depends on the respective boundary permeabilities, which in turn depend on the levels of aquaporin present; the model shows how changing the permeability of each boundary affects the emergence times (figure M6). It should be emphasised, however, that the system is fully coupled: changing one permeability alters the hydrostatic pressures, which affects how the other permeabilities influence the emergence time. We predict that increasing k_1^* (via an increase in $k_{1\text{init}}^*$) promotes emergence by increasing the flux into the primordium, whereas increasing k_3^* inhibits emergence by increasing the

flux away from the primordium (figure M6a). Increasing k_2^* (via an increase in $k_{2\text{init}}^*$) or k_4^* increases the flux into the overlaying tissue, leading to a higher pressure within the overlaying tissue that prevents the primordium from expanding and results in inhibited emergence (figure M6a). The permeabilities of boundaries 1 and 2 are also affected by auxin inhibiting the aquaporins (via parameters k_{jg}^*). Reducing k_{1g}^* and k_{2g}^* results in higher values of k_1^* and k_2^*, respectively; as shown in figure M6b, we see that reducing k_{1g}^* and k_{2g}^* has the opposite effect on emergence to reducing $k_{1\text{init}}^*$ and $k_{2\text{init}}^*$ (as one would expect from equation (1.8) and figure M4). Figure 4c in the main text summarises how auxin and the boundaries permeabilities affect the emergence time.

The simulations in figure M6 also reveal that the system exhibits switch-type behaviour, whereby a small change in one of the permeabilities causes a dramatic change in emergence time. Simulations show that the switch-type behaviour is due to sensitivity in the time at which boundary 1 yields. As shown in figure M7, a small change in one of the permeabilities causes a small change in the pressures of the two compartments. For example, with $k_{1\text{init}}^* = 2.5$, the primordium pressure becomes sufficiently greater than the overlaying-tissue pressure that boundary 1 yields at $t = 32.8$ hours; however, the small change in the pressures that occurs if we instead set $k_{1\text{init}}^* = 2.3$, results in the pressure difference not becoming large enough for yielding until $t = 77.0$ hours. This predicted switch-type behaviour may have significant biological implications: away from the critical permeability, small changes in the permeability would have little effect on the emergence time, whereas close to the critical level, a small change (in the right direction) would result in a dramatic delay to the emergence time. Since the permeabilities depend on the amount of aquaporin present, the switch-type behaviour corresponds to the emergence time depending on whether the aquaporin level is above or below a threshold value. Switches are commonly found in regulatory systems; this phenomenon would provide a biologically robust mechanism to enable the plant to control the timing of emergence (for example, via auxin regulating the aquaporins).

Figure M8 shows the sensitivity of the emergence times to the values of the remaining parameters. For these parameters, we find that switch-like behaviour does not occur close to their wild-type values suggested in Table 2. We find that increasing the rate, π_{1g}^*, at which the primordium's osmotic potential increases promotes emergence by increasing water fluxes to the primordium (figure M8a), whereas increasing the osmotic potential of the vasculature, π_{r1}^*, inhibits emergence by increasing water flow away from the primordium (figure M8b). Softening boundary 1 (leading to an increase in T^*, (2.2), via a rise in extensibility, ϕ_1), enables the primordium to grow more easily and the emergence time is reduced (figure M8c). With a larger boundary 1 yield stress, Γ_1^*, the pressure within the primordium must be larger before boundary 1 can lengthen, resulting in delayed emergence (figure M8d). Since boundary 2 remains stationary, its mechanical properties (characterised by ϕ_2^* and Γ_2^*) do not affect the emergence time. The emergence time also depends on the prescribed geometry of the tissue: if we reduce X_2^*, increase $\beta_1(0)$ or reduce $\beta_2(0)$, boundaries 1 and 2 are initially closer together, which leads to a reduction in the emergence time (figure M8e,f,g). Finally, we consider the influence of the distance between the two boundaries at which we suggest that emergence has occured, Y_m^*: reducing this distance delays emergence (figure M8h).

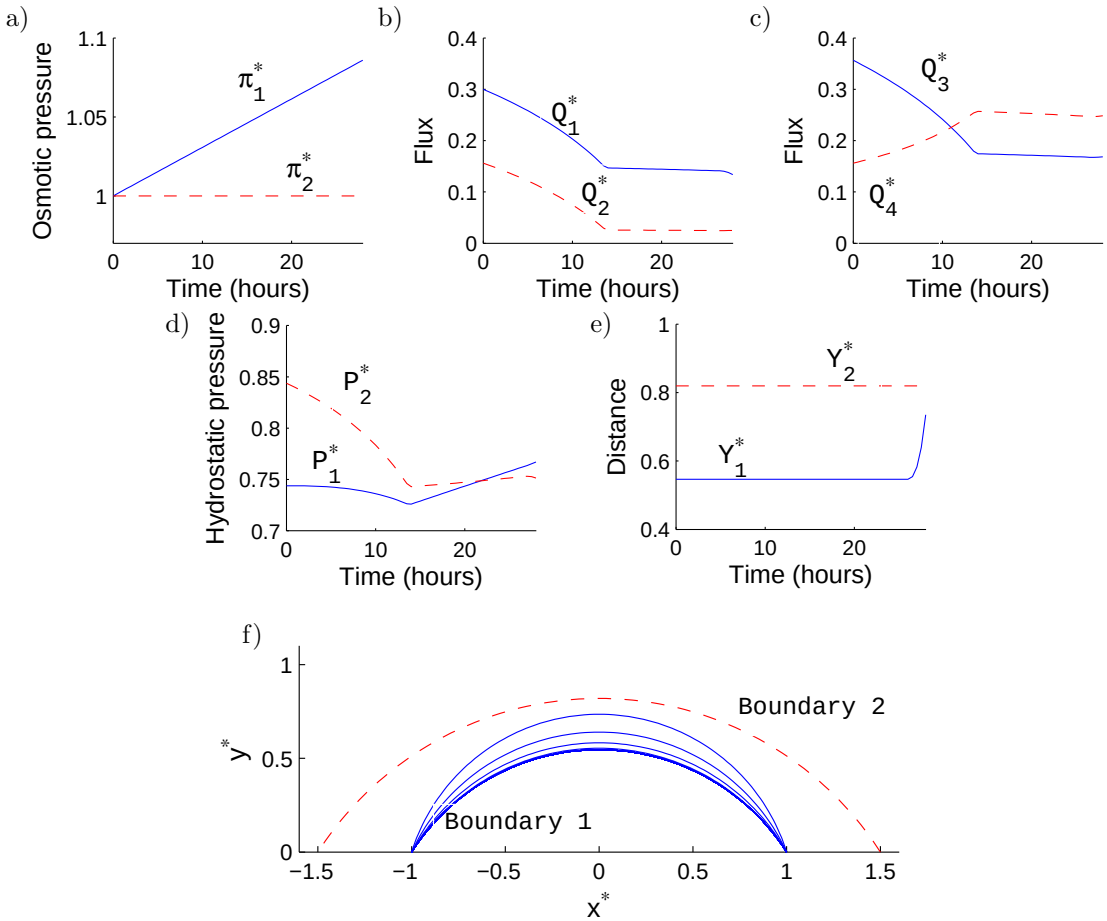

Figure M5: The emergence dynamics with the wild-type parameter values listed in Table 2 and $\beta_1(0) = \beta_2(0) = 1$. The subfigures show the evolution of a) the osmotic potentials of the primordium, $\pi_1^*(t)$, and the overlaying tissue, $\pi_2^*(t)$, b) the fluxes $Q_1^*(t^*)$ and $Q_2^*(t)$, c) the fluxes $Q_3^*(t)$ and $Q_4^*(t)$, d) the hydrostatic pressures, $P_j^*(t)$, e) the heights, $Y_j^*(t)$, and f) the boundary positions. In panel f), we show the position of boundary 1 at 0.5 hour intervals (blue lines) and the stationary position of boundary 2 (red dashed line). The primodium emerges at $t = 28$ hours.

a)

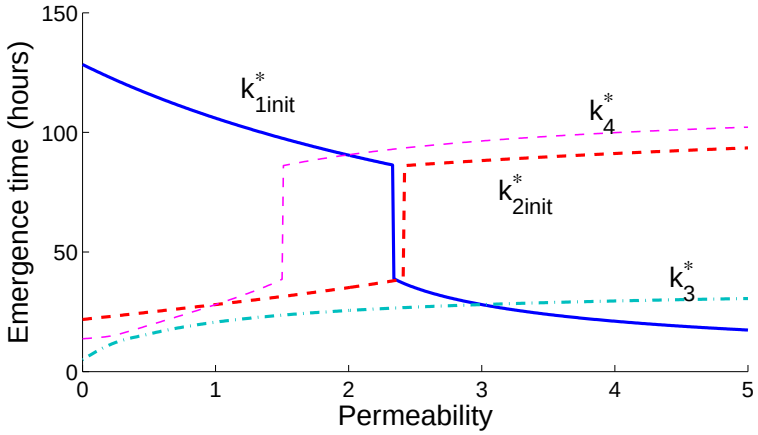

b)

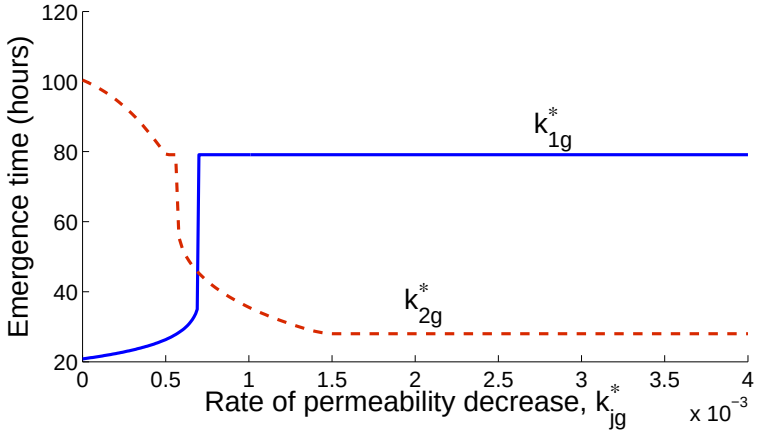

Figure M6: The influence of the permeability parameters on the predicted emergence time. In each case, the other parameter values are given in Table 2 and $\beta_1(0) = \beta_2(0) = 1$. a) The influence of the boundary permeabilities, $k^*_{j\text{init}}$, k^*_3 and k^*_4. Recall that during emergence the permeabilities of boundaries 1 and 2 gradually reduce from these initial values (see (1.8) and figure M4), whereas the permeabilities of boundaries 3 and 4 remain constant. When considering different $k^*_{j\text{init}}$, we set $k^*_{j\text{min}} = 0.1k^*_{j\text{init}}$ in each case. b) The influence of the rate of decrease of the permeabilities of boundaries 1 and 2, k^*_{jg}. These permeabilities gradually decrease during emergence because auxin causes a reduction the activity of the aquaporins.

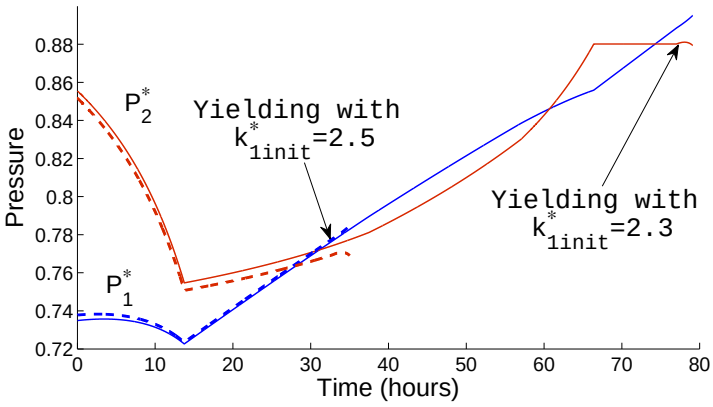

Figure M7: The evolution of the pressures in the primordium and overlaying tissue for $k^*_{1\text{init}} = 2.3$ (solid lines) and $k^*_{1\text{init}} = 2.5$ (dashed lines). In each case, boundary 1 yields once the pressure difference $P^*_1 - P^*_2$ is greater than $\Gamma^*_1 \sin(\beta_1(0))$; as shown with the arrows, with $k^*_{1\text{init}} = 2.5$ boundary 1 yields at 32.8 hours, whereas with $k^*_{1\text{init}} = 2.3$ boundary 1 yields at 77.0 hours. Thus, the small difference in the pressures between the two cases results in a significant difference in emergence time.

4.2 The influence of auxin on the emergence dynamics

As discussed above, auxin represses aquaporin expression and we capture this repression by prescribing a gradual reduction in the permeabilities of boundaries 1 and 2, at rates k^*_{1g} and k^*_{2g} respectively. Thus, from figure M6b, we see that auxin has opposing effects in the primordium and in the overlaying tissue. Considering boundary 1, auxin increases k^*_{1g}, which reduces the fluxes into the primordium from the overlaying tissue, inhibiting emergence. In contrast, considering boundary 2, auxin increases k^*_{2g}, which reduces the fluxes into the overlaying tissue, enabling the primordium to emerge more easily. With the parameter values stated in Table 2, we predict that neglecting the effects of auxin on either boundary has dramatic consequences for the emergence time; however, if we neglect auxin's influence entirely (*i.e.* removing its effect on both boundaries) the two opposing effects partly cancel each other, and we predict emergence to be only 8.7 hours later than wild-type (figure M9). However, since auxin has two opposing effects, the simulations reveal how the values of k^*_{1g} and k^*_{2g} affect whether setting $k^*_{1g} = 0$ dominates (resulting in earlier emergence when auxin's influence is removed) or whether setting $k^*_{2g} = 0$ dominates (causing delayed emergence when auxin's influence is removed). In particular, we predict a delay in emergence when we neglect auxin's influence entirely because auxin's inhibition of PIP2;1 (present on boundary 1) is slower than that of the other aquaporins (present on boundary 2) (so that the regions of rapid variation shown in figure M6b cause the change in k^*_{2g} to dominate). For example, if we consider auxin to have the same effect on the permeabilities of boundaries 1 and 2 by decreasing k^*_{2g}, *i.e.* $k^*_{1g} = k^*_{2g} = 5.6 \times 10^{-4}$ (and then adjust

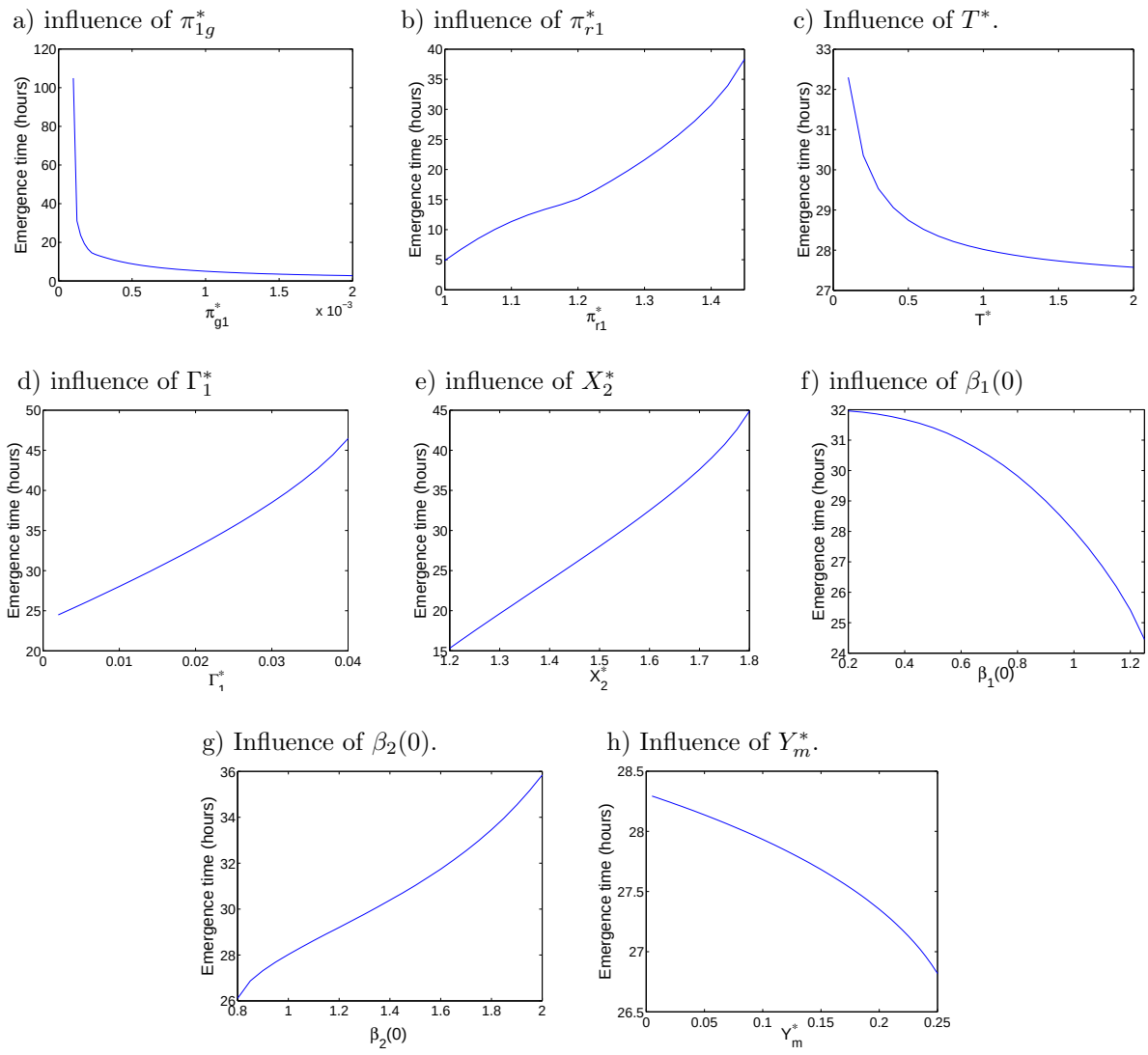

Figure M8: Influence of model parameters on the predicted emergence time. In each case, the remaining parameters are equal those given in Table 2 and $\beta_1(0) = \beta_2(0) = 1$.

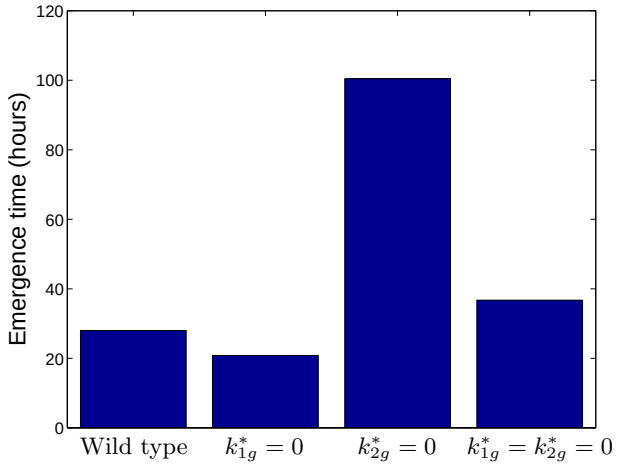

Figure M9: The influence of auxin on the predicted emergence time (via changes in the rates k^*_{1g} and k^*_{2g}). The remaining parameter values are given in Table 2 and $\beta_1(0) = \beta_2(0) = 1$.

	$k^*_{1\text{init}}$	k^*_{1g}	$k^*_{2\text{init}}$	k^*_{2g}	k^*_3	k^*_4	Emergence time
Wild type	3	5.6×10^{-4}	1	0.0028	3	1	28.02 hours
PIP2;1 overexpression	3	0	3	0	3	3	49.14 hours
pip2;1 knockout	0.6	0	1	0.0028	0.6	1	42.50 hours
Stele-specific PIP2;1	0.6	0	1	0.0028	3	1	57.94 hours
Primordium-specific PIP2;1	3	5.6×10^{-4}	1	0.0028	0.6	1	16.96 hours

Table 3: Summary of the permeability parameters used in simulating the differences in lateral root emergence in the wild type and mutant plants, together with the emergence times then predicted by the model.

$\pi^*_{g1} = 0.000206$ so that emergence still takes 28 hours in wild type), the model predicts that removing auxin's influence reduces the emergence time by 4 hours. Thus, the model suggests that differences in the rates at which auxin inhibits different aquaporins may have a significant effect on emergence. A detailed knowledge of the expression domains of different aquaporins would enable a more accurate assessment of auxins role; our results indicate that the relatively slow inhibition of PIP2;1 may be key to auxin promoting emergence.

In summary, the model suggests that auxin may be playing a key role in regulating the aquaporin distribution by adjusting the fluxes between different regions of the tissue.

4.3 The emergence dynamics in the mutants, *pip2;1* and d35S:PIP2;1

We now focus our attention on the spatial distribution of the aquaporin PIP2;1, and use the model to investigate the emergence dynamics in the *pip2;1* knockout mutant and the d35S;PIP2;1 over-expression mutant.

As described above, PIP2;1 is present in the stele and primordium prior to emergence; during emergence, PIP2;1 levels are maintained in the stele whilst auxin accumulation causes the PIP2;1 level in the primordium to reduce (see figure 3 in the main text). To assess whether this PIP2;1 distribution is important for emergence, we first simulate the emergence dynamics in the over-expression mutant, d35S;PIP2;1, by removing auxin's inhibition of the aquaporins and increasing the permeabilities of boundaries 2 and 4 (as detailed in Table 3). The model suggests that in the over-expression mutant the magnitudes of the fluxes Q_1^*, Q_2^* and Q_3^* are larger than in wild type (figure M10a,b). This results a larger difference between the pressures within the overlaying tissue and primordium, so that boundary 1 yields at a later time (figure M10c,d). Since the boundary's permeabilities are constant in this case, equations (2.8) can be manipulated to show that, prior to yielding, pressure P_2 is constant and pressure P_1 increases linearly with time. With the parameters stated in Table 3, emergence in the over-expression mutant is 21.1 hours later than in the wild type (figure M10d), in agreement with our experimental measurements, see figure 4e, main text. Considering the diagram in figure 4c, main text, we see when modelling the over-expression mutant, that increasing the permeabilities of boundaries 2 and 4 and removing auxin's inhibition of aquaporins on boundary 2 all have inhibitory effects on emergence, whereas removing auxin's inhibition of aquaporins on boundary 1 promotes emergence; the simulations reveal that the former effects dominate over the latter (in part due to the switch-like behaviour in the relationships between the permeabilities and emergence times shown in figure M6), resulting in the prediction of delayed emergence in the over-expression mutant. We note that predicting the experimentally observed delay requires us to set the permeabilities of boundaries 2 and 4 to be three times higher in the over-expression mutant than in wild type – if we only (say) double these permeabilities to represent the over-expression mutant, the model suggests emergence to be delayed by only 17.2 hours (when compared to wild type). Furthermore, expressing PIP2;1 under the control of the d35S promoter may also cause an increase in the permeabilities of boundaries 1 and 3, $k_{1\text{init}}^*$ and k_3^*, (where PIP2;1 is present in wild-type). Increasing these permeabilities could reduce the emergence time by allowing more water to flow from the overlaying tissue into the primordium (by increasing k_1^*, see figure 4c main text). However, if we represent the over-expression mutant by tripling the permeabilities of boundaries 1 and 3, $k_{1\text{init}}^* = k_3^* = 9$, as well as tripling the permeabilities of boundaries 2 and 4 (as detailed in Table 3), the model still predicts delayed emergence, although now only 8.5 hours later than wild type.

We also use the model to investigate the emergence dynamics in the *pip2;1* knockout mutant by removing auxin's repression of boundary 1's permeability and reducing the permeabilities of boundaries 1 and 3 (see Table 3). The diagram in figure 4c, main text, shows that these perturbations have opposing effects on emergence: reducing the permeability of boundary 1 inhibits emergence, whereas emergence is promoted by reducing the permeability of boundary 3 and removing auxin's inhibition of boundary 1's permeability. Thus, the modelling suggests that with tissue-specific knockouts, knocking out PIP2;1 in the primordium

(*i.e.* stele-specfic PIP2;1 expression) would delay emergence whereas knocking out PIP2;1 in the stele (*i.e.* primordium-specfic PIP2;1 expression) would result in faster emergence (see Table 3). Considering the space of possible parameter values, with PIP2;1 knocked out in both the primordium and the stele, the model consistently predicts that the change in the permeability of boundary 1 is the dominant effect (due to the switch-like behaviour shown in figure M6) and so emergence is delayed in the *pip2;1* mutant. The simulations suggest that the magnitudes of the fluxes are smaller than those in wild type (figure M11a,b). However, as in the over-expression mutant, this results in a larger difference between the pressures of the primordium and overlaying tissue, so emergence is again delayed (figure M11c,d). Furthermore, with the parameter values suggested in Table 3, the simulated and measured emergence times for *pip2;1* are in good agreement and both suggest a delay of about 15 hours (see figure 4e, main text). As for the over-expression mutant, the magnitude of the delay does, however, depend on our parameter choice. For instance, if we assume k_1^* and k_3^* to be reduced only by a factor of three in the *pip2;1* mutant, the model predicts that emergence is 7.5 hours later than in the wild type. In addition, the delay also relies on us setting k_1^* and k_3^* to be relatively high in wild type (as mentioned in section 3), so that reducing these parameters has a significant effect on emergence time (*cf.* the relationships between these permeabilities and the predicted emergence times shown in figure M6). If instead we assume that all the permeabilities are equal in wild type (and adjust π_{g1}^* to 0.000226 so that emergence in wild type takes 28 hours), the model predicts that emergence is delayed by only 4.4 hours in the *pip2;1* mutant.

In summary, the model predicts that emergence is inhibited in both the knockout mutant and the over-expression mutant. While this result appears at first sight to be highly counterintuitive, the model provides an explanation. In the over-expression mutant, water fluxes into the overlaying cells are higher, inhibiting the primordium's expansion, whereas in the knockout mutant, water fluxes into the primordium are lower, resulting in a slower expansion of the primordium. While a number of the parameter choices are unclear, varying these parameters does not affect our key conclusion that emergence is delayed in both mutants. As described in the main text, we tested this prediction by measuring the emergence time in both mutants (by synchronising lateral root initiation using a gravitropic stimulus), these data validating our model conclusions. Furthermore, we found that the model could accurately predict the observed emergence times using appropriate parameter values. Thus, the model and experimental validation show that the wild-type PIP2;1 distribution is key to efficient emergence.

4.4 Water flux rates

We present a tissue-scale model, supposing for simplicity, that the boundaries lengthening and water fluxes occur over similar time scales (setting parameter grouping $T^* = 1$). Therefore, aquaporins regulate the rate at which water flows and alters the hydrostatic pressures on the time scale of emergence. Whether this assumption is appropriate at the tissue scale remains to be determined, and therefore, as mentioned in §3, we now discuss the implications of an alternative assumption in which the rate at which the boundaries lengthen is much smaller than that of the water fluxes ($\phi_1 \ll k_{\mathrm{typ}}/X_1^2$). In this case, parameter grouping

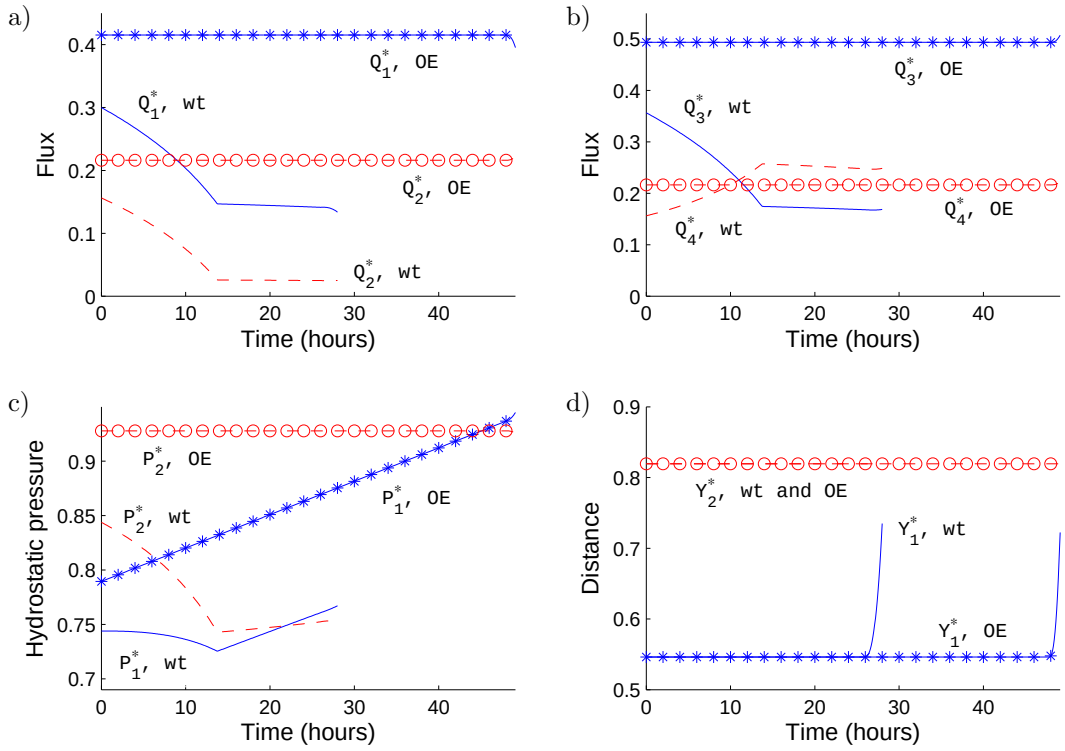

Figure M10: Comparing the predicted emergence dynamics in wild type (wt) and in the d35S:PIP2;1 over-expression mutant (OE). The permeabilities in each case are detailed in Table 3, the remaining parameter values are given in Table 2 and $\beta_1(0) = \beta_2(0) = 1$. The subfigures show a) the fluxes $Q_1^*(t^*)$ and $Q_2^*(t)$, b) the fluxes $Q_3^*(t)$ and $Q_4^*(t)$, c) the pressures, $P_j^*(t)$, and d) the heights, $Y_j^*(t)$.

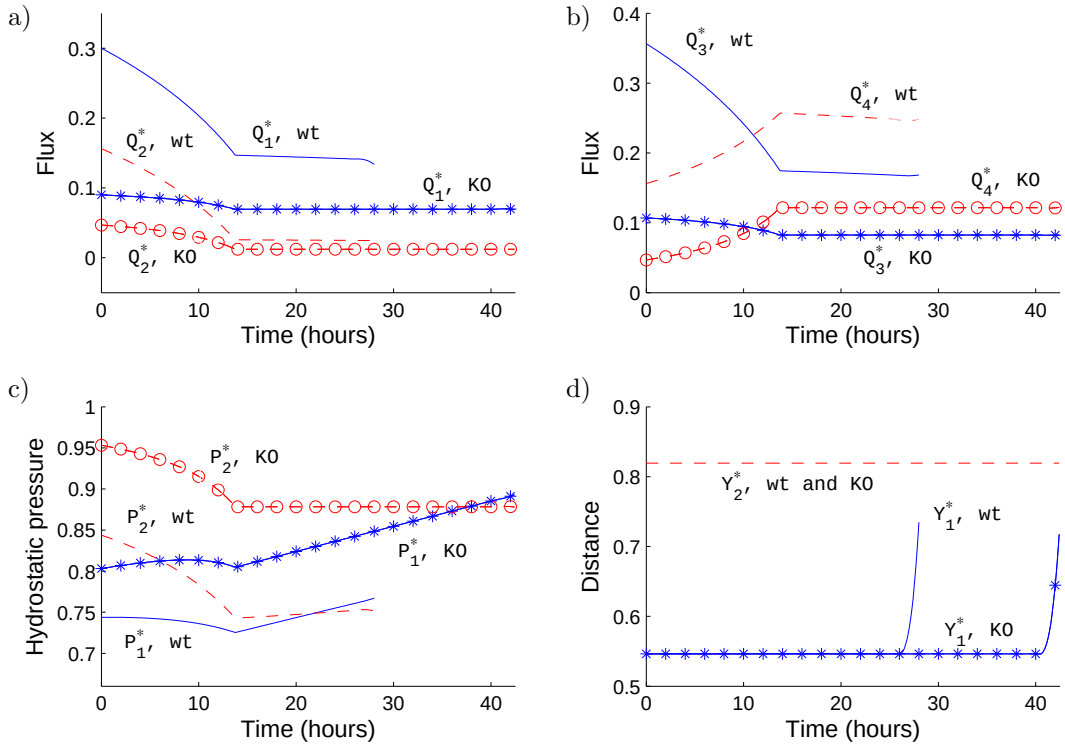

Figure M11: Comparing the predicted emergence dynamics in wild type (wt) and in the *pip2;1* knockout mutant (KO). The permeabilities in each case are detailed in Table 3, the remaining parameter values are given in Table 2 and $\beta_1(0) = \beta_2(0) = 1$. The subfigures show a) the fluxes $Q_1^*(t^*)$ and $Q_2^*(t)$, b) the fluxes $Q_3^*(t)$ and $Q_4^*(t)$, c) the pressures, $P_j^*(t)$, and d) the heights, $Y_j^*(t)$.

$T^* \ll 1$ and from (2.5c,d), we see that the hydrostatic pressures in the primordium and overlaying tissue are in quasi-equilibrium, with their relative sizes dependent on the aquaporin distribution (via the permeability parameters k_j^*). These hydrostatic pressures affect the rate at which the primordium expands (via (2.5a,b)), and hence the timing of lateral root emergence. Key to this phenomenon is the high osmotic potential within the sap driving a continual water flux from the region external to the root to the stele. Due to this flux, the relative permeabilities of the boundaries affect the relative drops in hydrostatic pressures between the overlaying tissue and the primordium regions and hence the aquaporin distribution regulates water potential gradients between different regions of the tissue.

To verify this reasoning and whether our conclusions hold if the boundaries lengthen more slowly, we performed model simulations with small values of T^*. As shown in figure M8, reducing T^* leads to delayed emergence. Considering $T^* = 0.01$, for example, we increase π_{1g}^* to 0.000217 to ensure emergence occurs after 28 hours in wild-type plants; as in the original model results (with $T^* = 1$), we predict delayed emergence in the cases of (i) removal of the influence of auxin ($k_{1g}^* = k_{2g}^* = 0$, 34.64 hours), (ii) the d35S:PIP2;1 mutant (42.22 hours) and (iii) the *pip2;1* knockout mutant (37.82 hours) (using the parameter values listed in Tables 2 and 3). Similar delays are also predicted with other small values of T^*. These results suggest that our conclusions are not affected by our choice of time scale at which the boundaries lengthen.

References

Bressan, R.A., Handa, A.K., Handa, S. and Hasegawa, P.M. 1982. Growth and water relations of cultured tomato cells after adjustment to low water potentials. *Plant Physiol.* **70**, 1303–1309.

Boyer J.S. and Silk W.K. 2004. Hydraulics of plant growth. *Funct. Plant Biol.* **31**, 761–773.

Cosgrove, D.J. 1993. Water uptake by growing cells: an assessment of the controlling roles of wall relaxation, solute uptake and hydraulic conductance. *Int. J. Plant Sci.* **154**, 10–21.

Dumais, J. and Forterre, Y. 2012. "Vegetable Dynamicks" The role of water in plant movements. *Annu. Rev. Fluid Mech.* **44**, 453–478.

Dyson, R.J. and Jensen, O.E. 2010. A fibre-reinforced fluid model of anisotropic plant root cell growth. *J. Fluid Mech.* **655**, 472–503.

Javot, H. and Maurel, C. 2002. The role of aquaporins in root water uptake. *Ann. Bot.* **90**, 301–313.

Javot, H., Lauvergeat, V., Santoni, V., Martin-Laurent, F., Guclu, J., Vinh, J., Heyes, J., Franck, K., Schäffner, A.R., Bouchez, D., Maurel, C. 2003. Role of a single aquaporin isoform in root water uptake. *Plant Cell* **15**, 509–522.

Kramer P.J. and Boyer J.S. 1995. Water relations of plants and soils. *Academic Press, Orlando*

Lockhart, J.A. 1965 An analysis of irreversible plant cell elongation. *J. Theor. Biol.* **8**, 264275.

Malamy, J.E. and Benfey P.N. 1997. Organization and cell differentiation in lateral roots of *Arabidopsis thaliana*. *Development* **124**, 33-44.

Murphy, R. 2000. Some compartmental models of the root: steady state behaviour. *J. Theor. Biol.* **207**, 557-576.

Murphy, R. 2003. Steady-state water relations of soybean seedling roots. *Funct. Plant Biol.* **30**, 377-389.

Postaire, O., Tournaire-Roux, C., Grondin, A., Boursiac, Y., Morillon, R., Schäffner, A.R. and Maurel, C. 2010. A PIP1 aquaporin contributes to hydrostatic pressure-induced water transport in both the root and rosette of *Arabidopsis*. *Plant Physiol.* **152**, 1418-1430.

Swarup, K., Benková, E., Swarup, R., Casimiro, I., Péret, B., Yang, Y., Parry, G., Nielsen, E., De Smet, I., Vanneste, S., Levesque, M.P., Carrier, D., James, N., Calvo, V., Ljung, K., Kramer, E., Roberts, R., Graham, N., Marillonnet, S., Patel, K., Jones, J.D.G., Taylor, C.G., Schachtman, D.P., May, S., Sandberg, G., Benfey, P., Friml, J., Kerr, I., Beeckman, T., Laplaze, L. and Bennett, M.J. 2008. The auxin influx carrier LAX3 promotes lateral root emergence. *Nat. Cell Biol.* **10**, 946–954.

Van der Fliert, B.W., Howell, P.D. and Ockendon, J.R. 1995. Pressure-driven flow of a thin viscous sheet. *J. Fluid Mech.* **292**, 359–376.